Supporting information for

Rapid and selective removal of toxic and radioactive anionic pollutants using an ionic covalent organic framework (iCOF-2)

Atikur Hassan,[†] Md Mofizur Rahman Mollah,[§] Soumen Das,[§] Neeladri Das[*†]

†Department of Chemistry, Indian Institute of Technology Patna, Patna 801106, Bihar, India

§ Materials Chemistry and Metal Fuel Cycle Group, Indira Gandhi Centre for Atomic Research, Kalpakkam 603 102, Tamil Nadu, India

Corresponding Author. E-mail: neeladri@iitp.ac.in, neeladri2002@yahoo.co.in

Tel.: +91 9631624708

Table of Contents

Section S1

Raw Materials: Resorcinol, guanidinium chloride and hydrazine hydrate were procured from Merck. All the other reagents and solvents were purchased locally and were used as obtained without further purification. Distilled water was used for all the capture experiments, unless otherwise specified. Water samples from various sources (such as tannery, pond, lake and river) were collected from industrial and rural areas of Kolkata, India. A sample of sea-water was collected from Chennai (Marina beach), India.

Characterization:

Fourier transform infrared spectra (FTIR) of samples were collected using the ATR mode of a PerkinElmer 400 FT-IR spectrophotometer. Solid-state ^{13}C CP-MAS NMR spectrum of iCOF-2 was recorded with 400 MHz Bruker NMR instrument. Solution phase NMR were also recorded on 400 MHz Bruker NMR. Powder X-ray diffraction (P-XRD) patterns were obtained using a GNR XRD with Cu Kα radiation (α = 1.5406 Å) at a scan rate of 2°/min. Thermogravimetric analysis (TGA) of iCOF-2 samples were performed by using a SDT Q600 (TA Instruments) equipment. The experiments were carried out in the temperature range of 30−700 °C, under nitrogen atmosphere with regulated heating rate of 10°C/min. The porous nature of the material and its surface area were determined using Quantachrome Autosorb iQ_2 instrument (Quantachrome, USA). Prior to analysis, a given sample was activated at 120 °C for 12h. Following activation, the sample was subjected to gas adsorption measurements (P/P_0 range from 0 to 1 atm.) at 77 K. The Brunauer-Emmett-Teller (BET) model was employed for the calculation of the specific surface area of iCOF-2. The distribution of pore size was obtained from the nitrogen gas sorption curves utilizing the non-local density functional theory (NL-DFT). Zeta-potential data was obtained using Anton Paar Lite sizer 500 with 100 runs (manual mode). Morphological studies were done using a ZEISS Field Emission Scanning Electron Microscope (FE-SEM). Before analysis, the samples were sputter-coated with gold. A voltage of 20 kV was applied to perform elemental analyses and mapping with energy dispersive elemental analysis technique (EDX). Atomic Force Microscope (AFM) images were taken using an Agilent instrument. Irradiation experiments for iCOF-2 samples were performed at various dose levels such as 50 kGy, 100 kGy, 200 kGy and 300 kGy for 3.2 days, 6.4 days, 12.8 days and 19.2 days respectively. UV-visible absorption spectra were recorded on a Shimadzu UV-2550 UV-vis spectrophotometer. Raman spectra were obtained using a laser of 532 nm on a Renishaw Ramanscope system (micro-Raman spectrometer). All the images reported herein were captured using Canon DSLR or Motorola moto g60 mobile camera.

Section S2

Synthesis of triformylresorcinol (TFR)[1] -

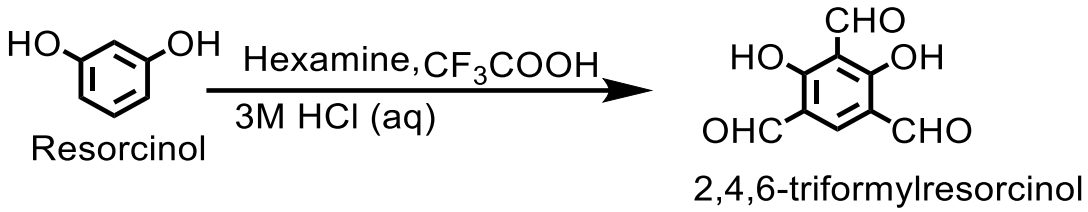

A mixture of resorcinol (1g, 9.1 mmol) and hexamine (HMTA: hexamethylenetetramine) (2.79 g, 19.9 mmol) were dissolved in 15 mL trifluoroacetic acid (TFA) under an argon atmosphere. The reaction mixture was refluxed at 120 °C for 24 h, and then heated at 150 °C for additional 3h. Subsequently, the reaction mixture was cooled to 100 °C and treated with 20 mL 3M HCl. After the addition of HCl, the formation of a yellow precipitate was observed within 5 minutes. Reaction mixture was heated for additional 30 minutes at 120 °C. The crude products thus obtained were filtered and washed repeatedly with ethanol until the filtrate was clear. The desired product was obtained as a powder after drying in oven at 60 °C for several hours.

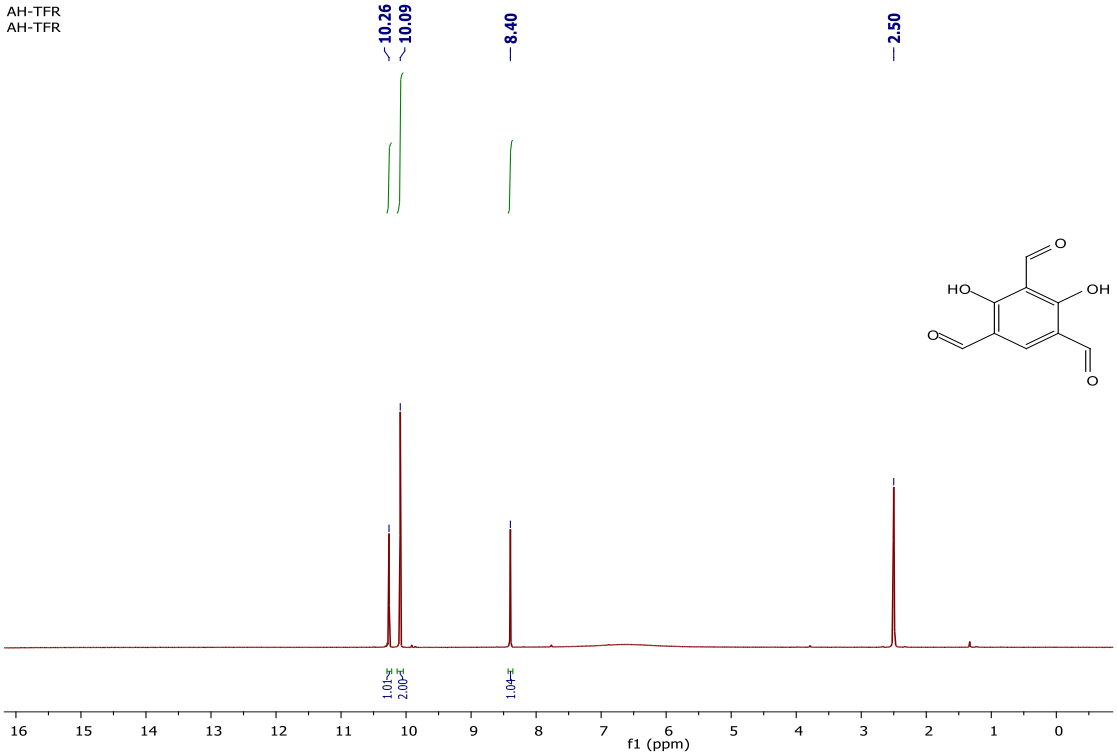

Fig. S1: ^{1}H NMR of the TFR

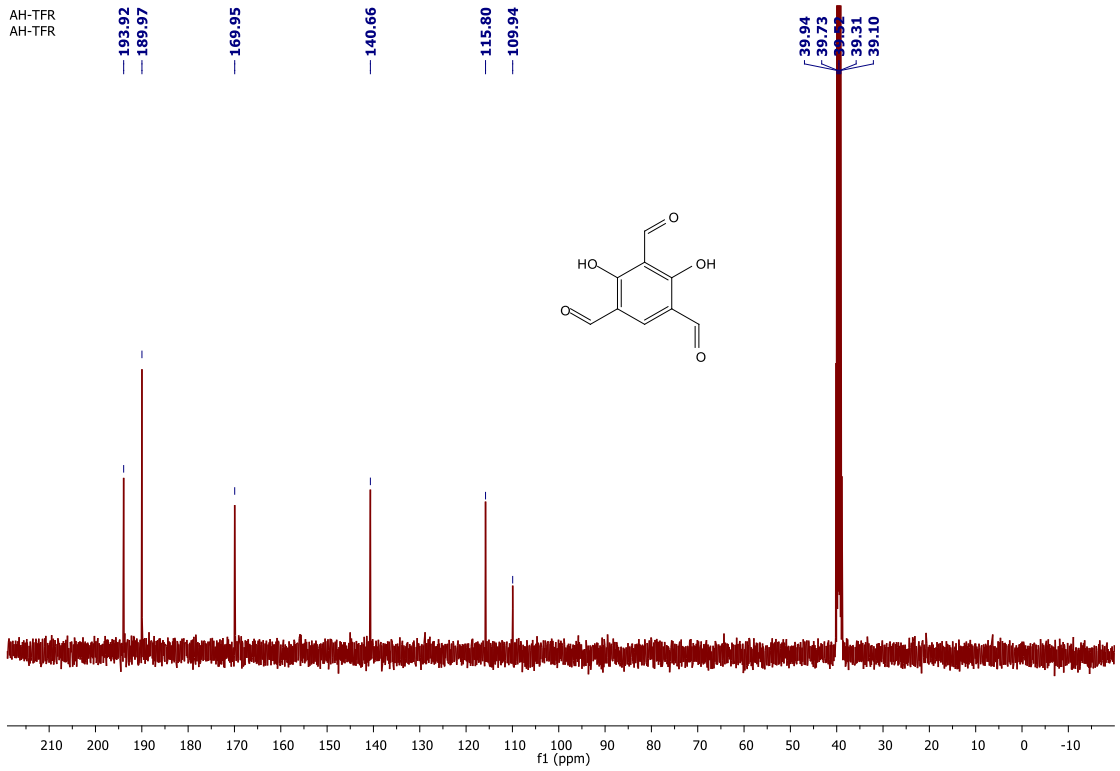

Fig. S2: $^{13}C\{^{1}H\}$ NMR of the TFR

Synthesis of triaminoguanidium chloride $(TAG_{Cl})^{2}$-

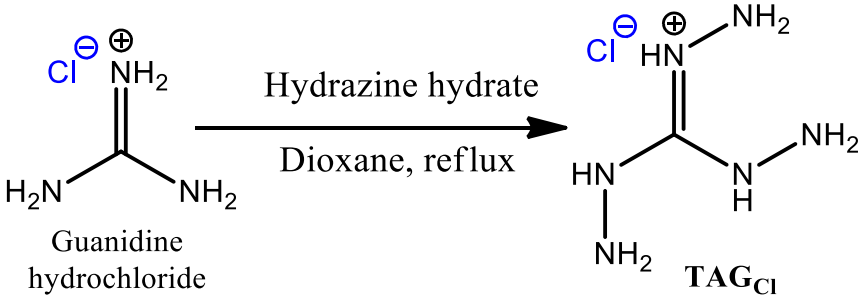

To a mixture of 1.91 g (20 mmol) guanidine hydrochloride and 3.41 g (106 mmol) hydrazine hydrate, 10 ml of 1,4-dioxane was added while stirring continuously. The mixture was refluxed for 2 hours. The reaction mixture was then allowed to cool to room temperature and the product was filtered. The product was then washed with 1,4-dioxane and dried to give triaminoguanidinium chloride (TAG_{Cl}).

Synthesis of iCOF-2

1,3,5-triformylrecorcinol benzene (42 mg, 0.2 mmol) and triaminoguanidinium chloride (28 mg, 0.2 mmol) were dissolved in solvent containing 2:0.6 v/v ratio of 1,4 Dioxane and water with continuous stirring. Later, the reaction mixture was charged into a Pyrex tube and

sonicated for 10 min. The reaction mixture was maintained at 120 °C for 3 days and later cooled to room temperature. iCOF-2 was obtained as dark yellow precipitate (57 mg).

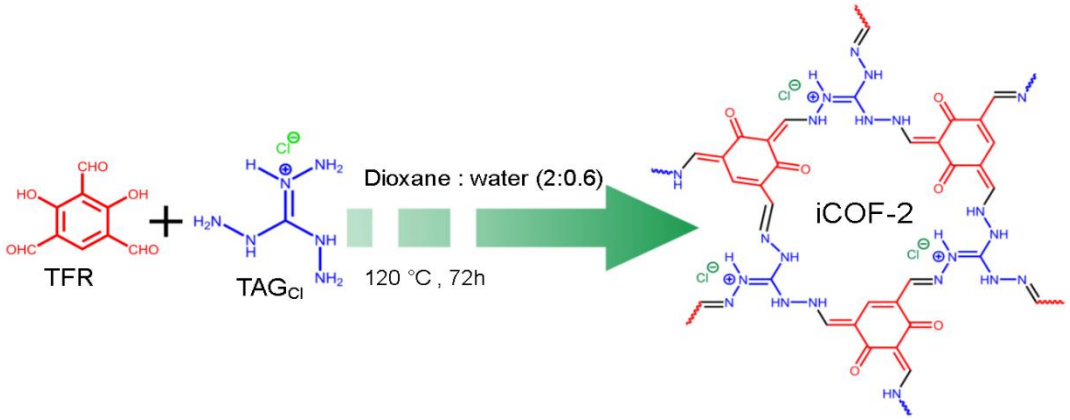

Synthesis of Sa-TAG$_{Cl}$ monomer [2] (model compound)

Triaminoguanidinium chloride (2.34 g, 0.017 mol) was dissolved in a hot mixture of ethanol (54 mL) and water (27 mL). A solution of 2- hydroxybenzaldehyde (0.05 mol) in ethanol was slowly added to it. The resulting mixture was refluxed and the precipitate of Sa-TAG$_{Cl}$ model compound [N',N",-2-tris((E)-2-hydroxybenzylidene)hydrazine1-carbohydrazonhydrazide hydrochloride] was collected accordingly. The precipitate was washed with acetone and dried under reduced pressure. The obtained product (Sa-TAG$_{Cl}$) was characterized using FT-IR and NMR spectroscopy.

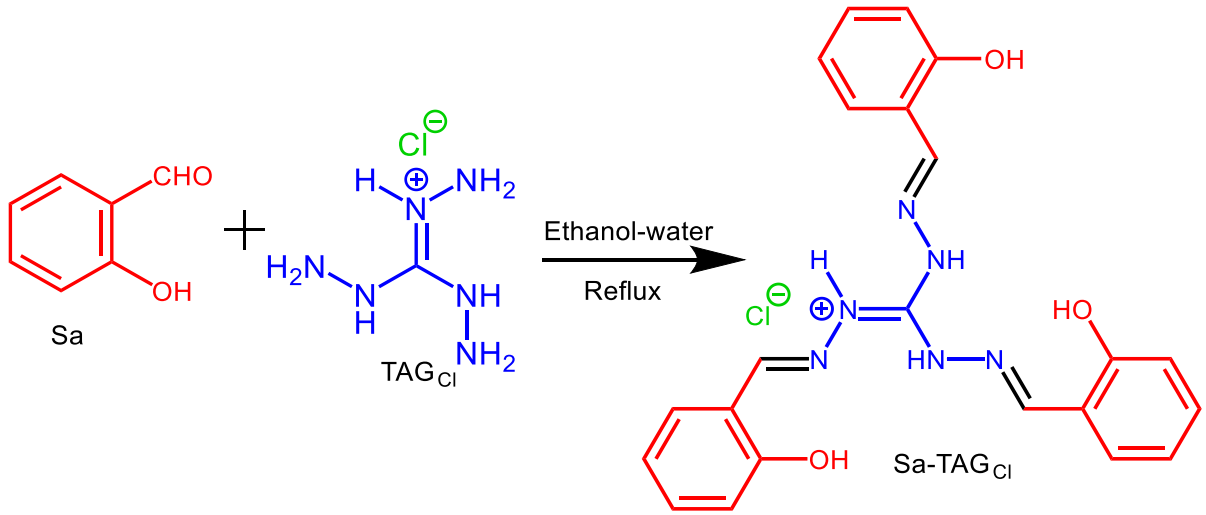

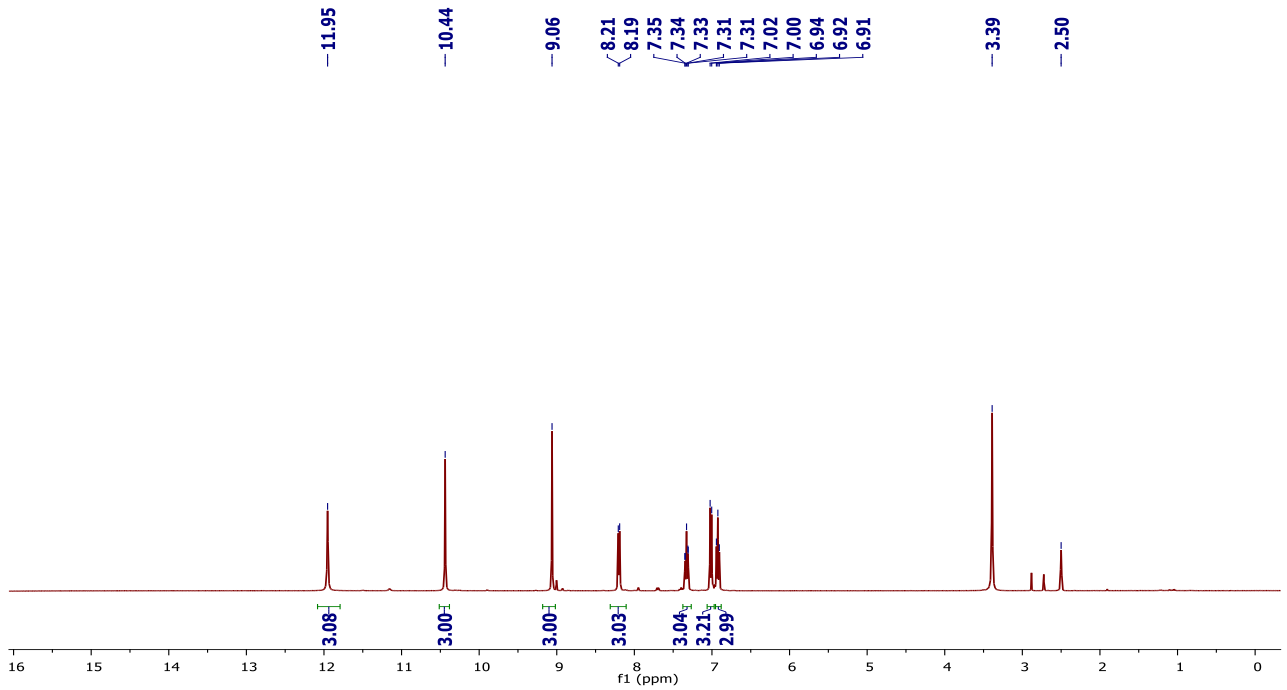

Fig. S3: ^{1}H NMR of Sa-TAG$_{Cl}$

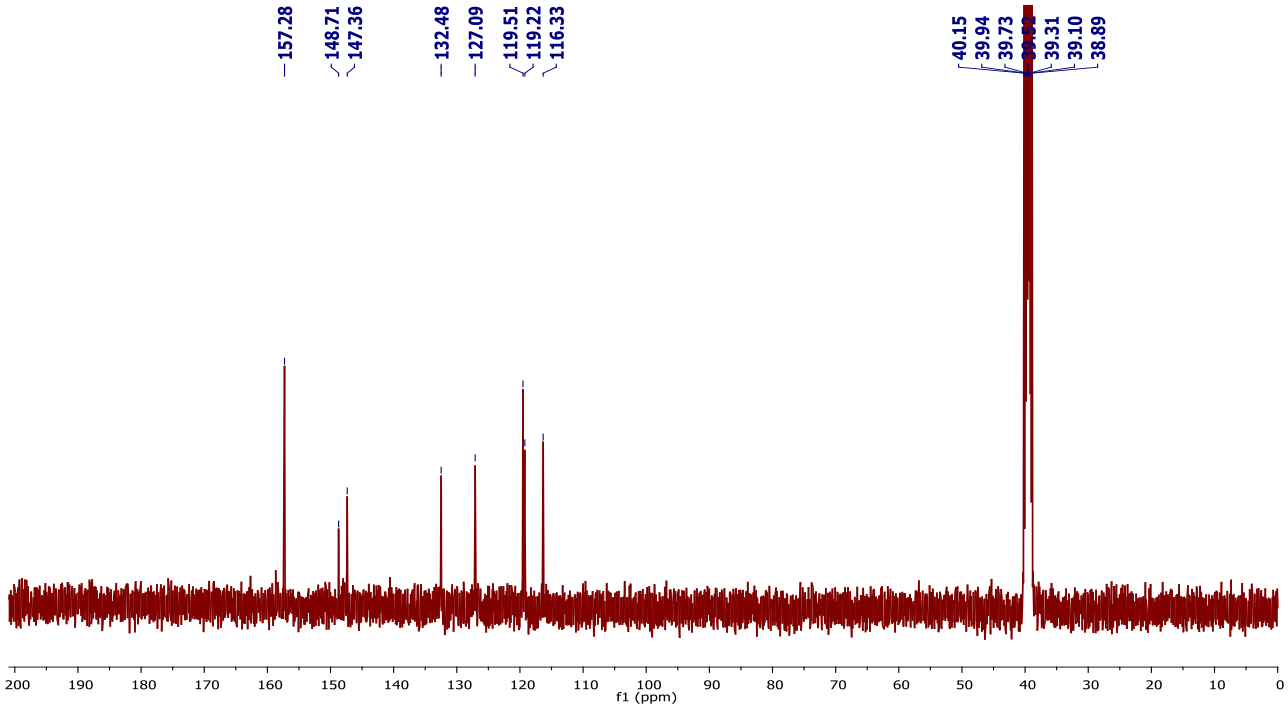

Fig. S4: ^{13}C{^{1}H} NMR of Sa-TAG$_{Cl}$

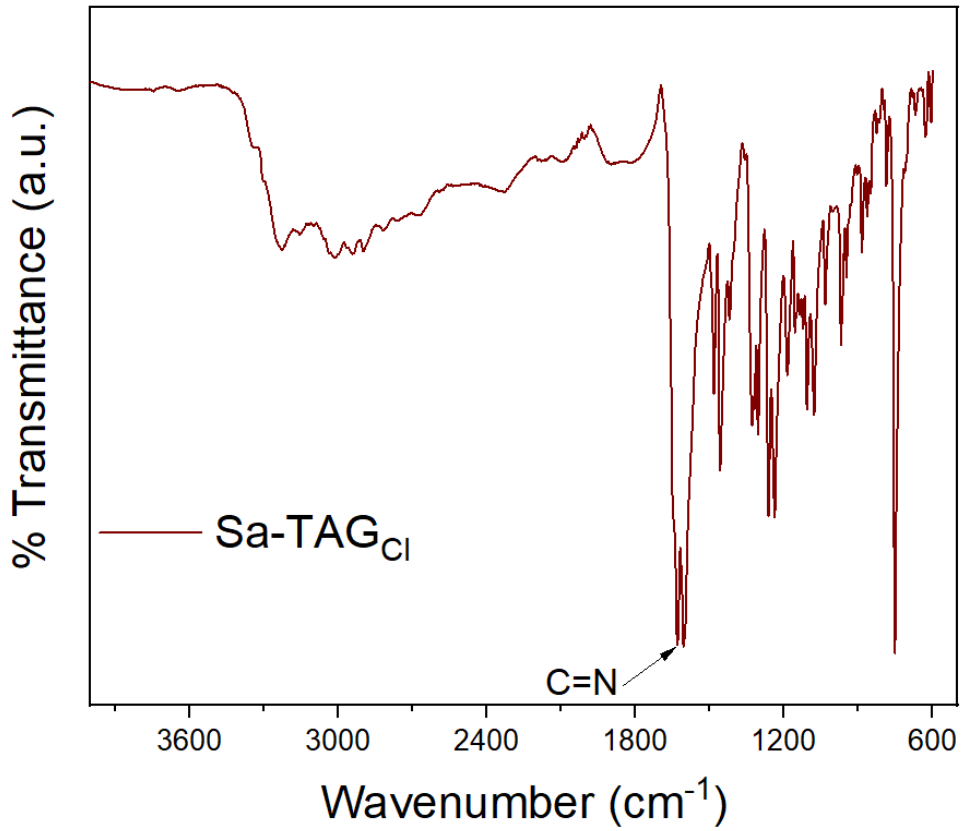

Fig. S5: FTIR spectrum of Sa-TAG$_{Cl}$

Section S3

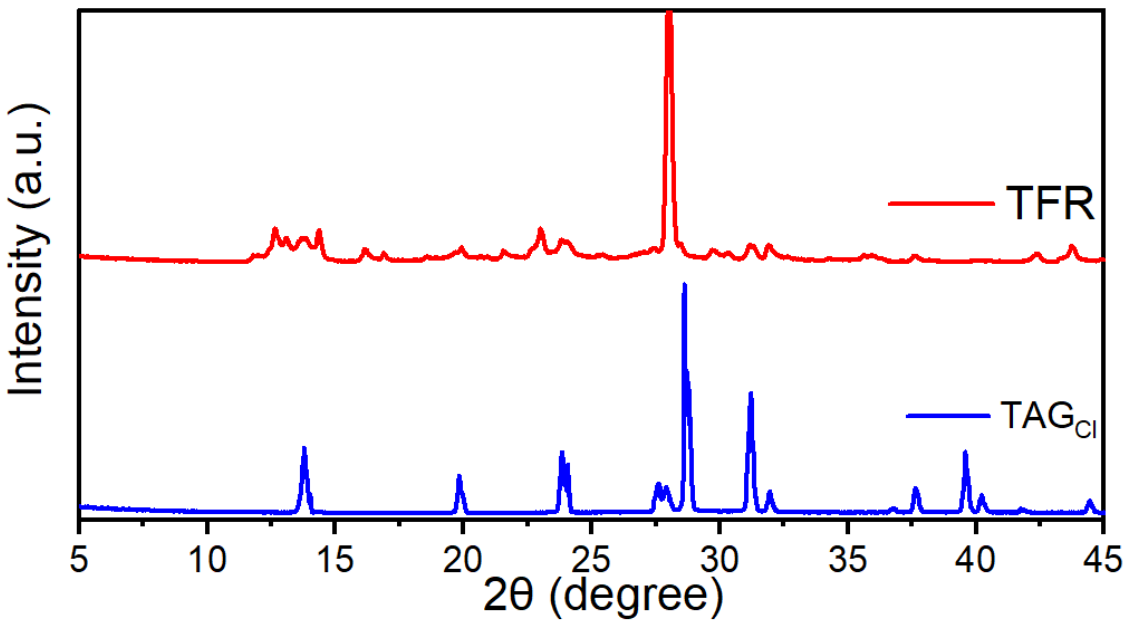

Fig. S6: P-XRD of monomers

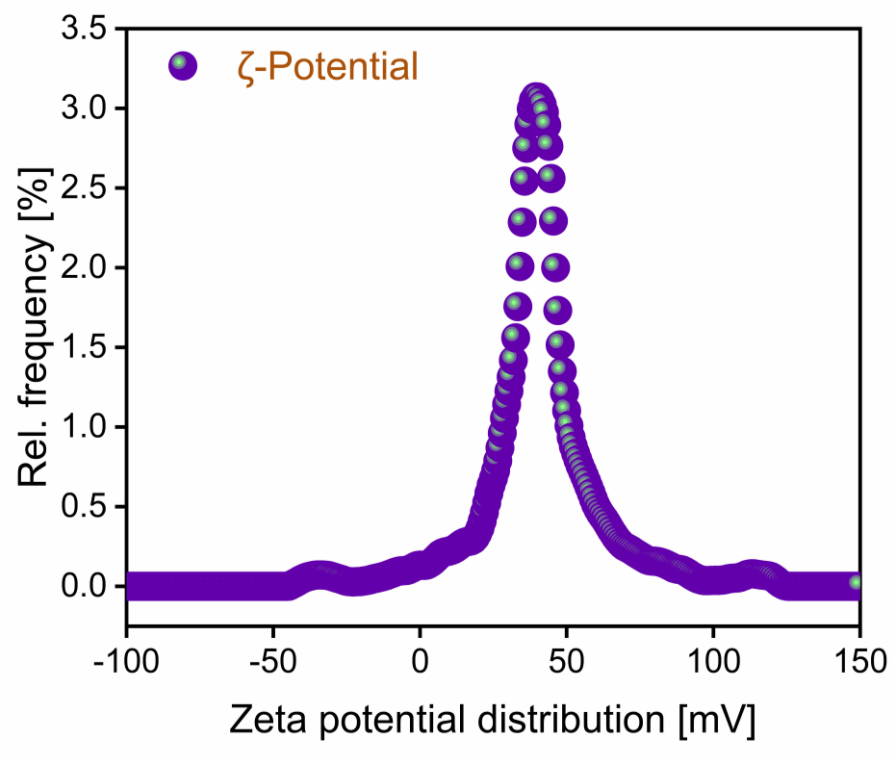

Fig. S7: Zeta potential analysis of iCOF-2

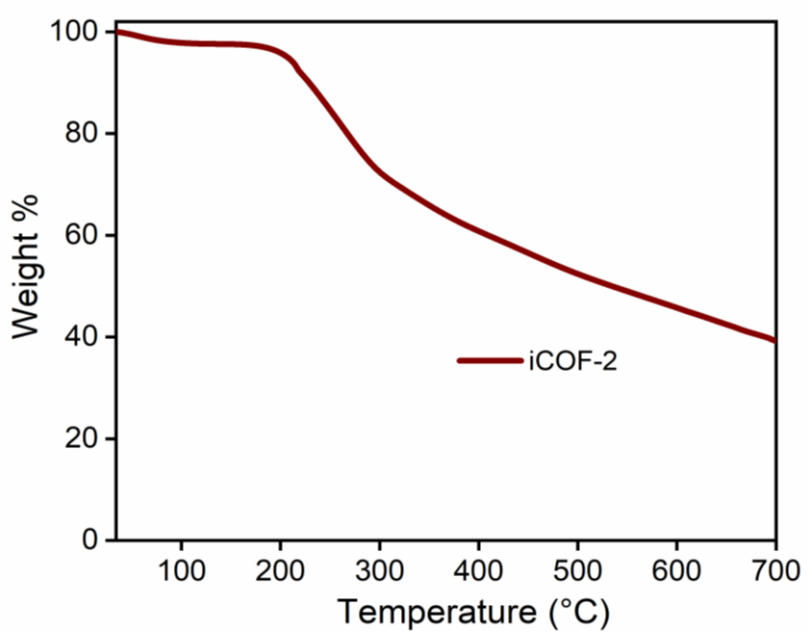

Fig. S8: TGA thermogram of iCOF-2

Table -S1: Comparison of BET surface area: (iCOF-2 vs literature reported iCOFs /iCONs)

Name of the compounds	BET Surface area (m^2/g)	References
iCOF-2	306.86	**This work**
CON-Cl	220	*J. Am. Chem. Soc.* **2018**, 140, 896−899
$TpTG_{Cl}$	267	*J. Am. Chem. Soc.* **2016**, 138, 2823−2828
$DATG_{Cl}$-iCONs	155	*ACS Appl. Mater. Interfaces* **2020**, 12, 13248−13255
TGH+•PD	16	*Nat Commun.* **2022,** 13, 3904
BT-DG_{Cl}	3	*Environ. Sci. Technol.* **2019**, 53, 878−883
ICOP-1	198	*ACS Sustainable Chem. Eng.* **2019**, 7, 1564−1573
POF1	200	*Chem. Sci.*, **2020**,11,7910–7920
TFPB–TG_{Cl}–iCOF TFPT–TG_{Cl}–iCOF	228 454	*J. Mater. Chem. A*, **2020**,8,12657–12664
TG-DFP	53	*Chem. Mater.* **2019**, 31, 4148−4155
IPOF-Cl	163	*Nanoscale*, **2021**,13,3967–3973
$BdaTG_{Cl}$	66.3	*Chem. Eng. J*, **2022**, 428131124
$DhaTG_{Cl}$	96	*Environ. Sci. Technol.* **2019**, 53, 5212−5220
iCON - I	12.50	*ACS Appl. Nano Mater.* **2021**, 4, 12, 13319–13328
COFTGTp	152.8	*J. Hazard. Mater.*, **2022** 435 128965

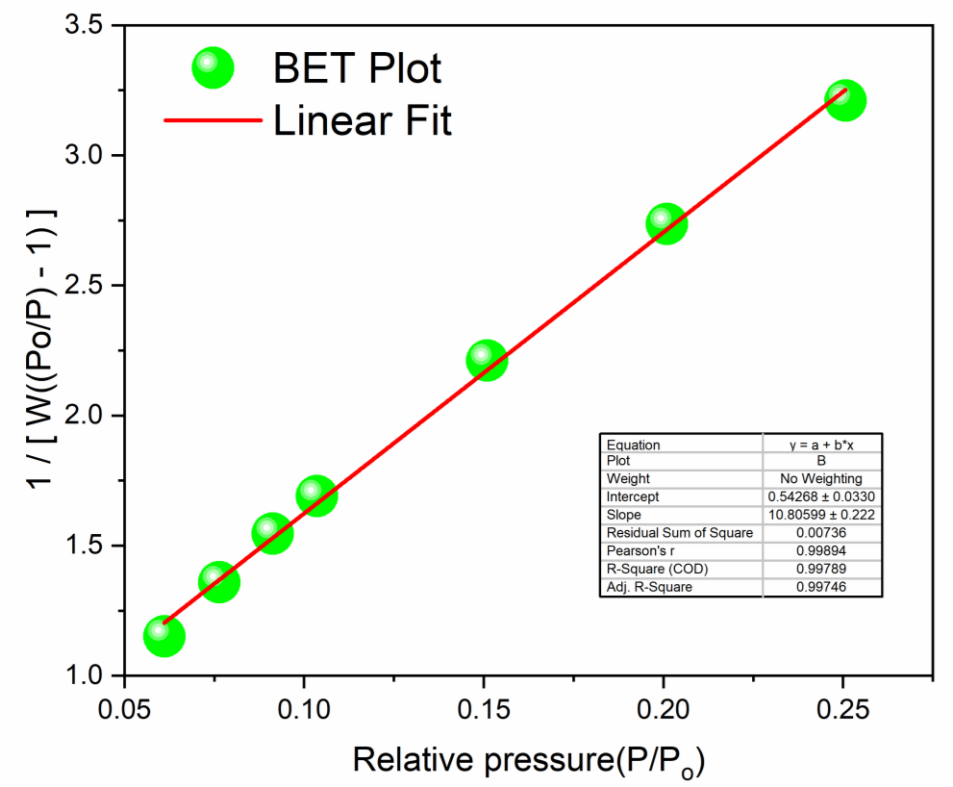

Fig. S9: BET plot of iCOF-2

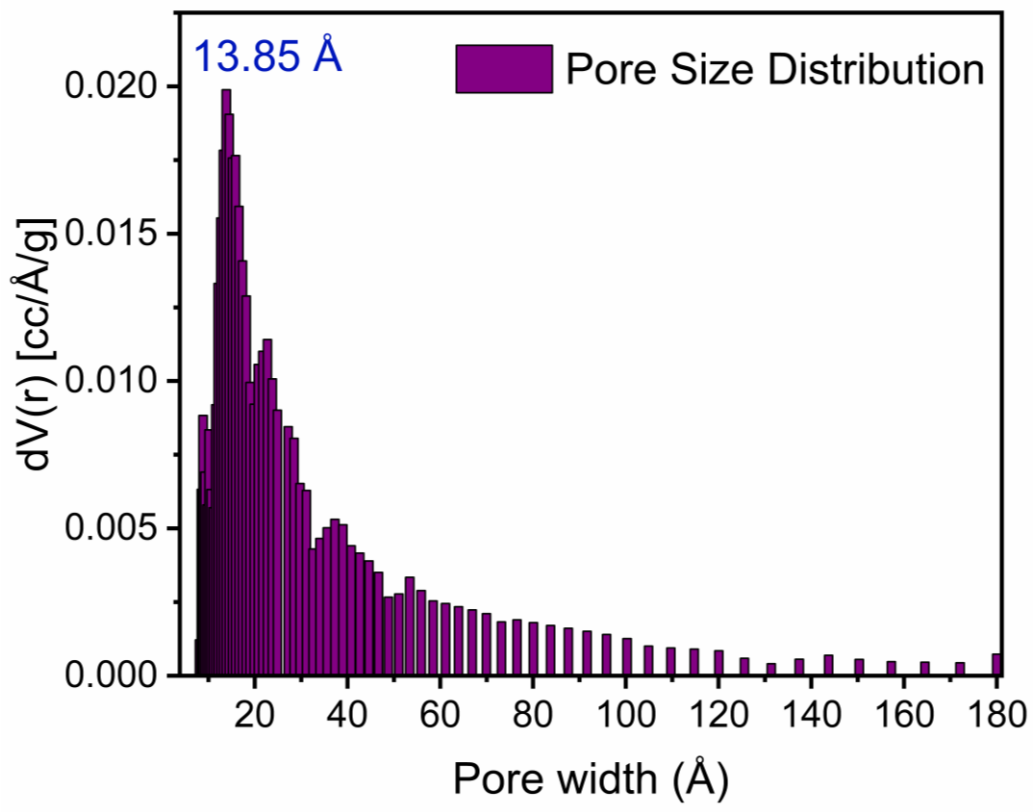

Fig. S10: Pore size distribution of iCOF-2

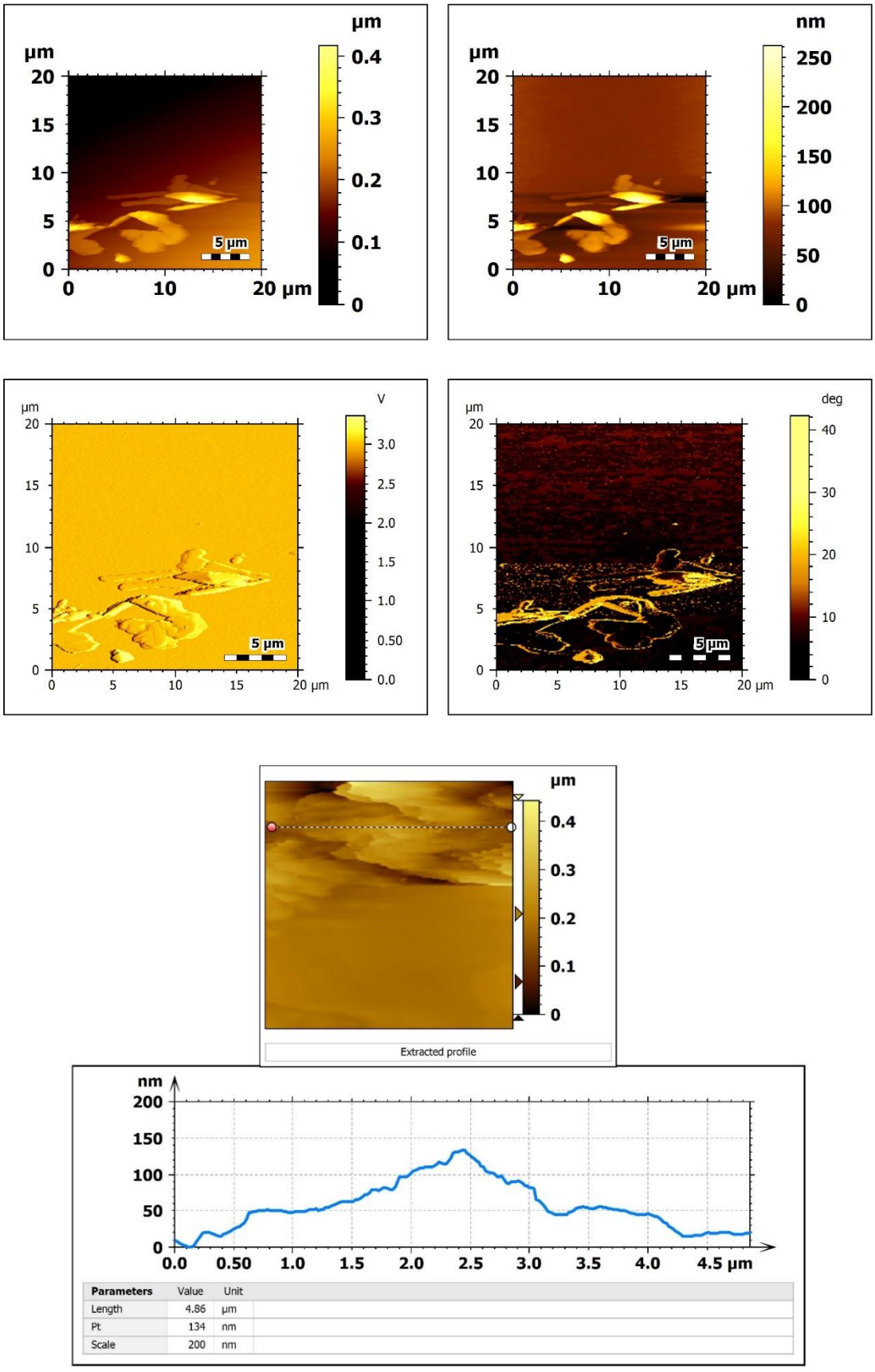

Fig. S11: AFM micrographs of iCOF-2

Element	Weight%	Atomic%
C K	53.71	59.41
N K	26.39	25.03
O K	17.79	14.77
Cl K	2.12	0.79
Totals	100.00	

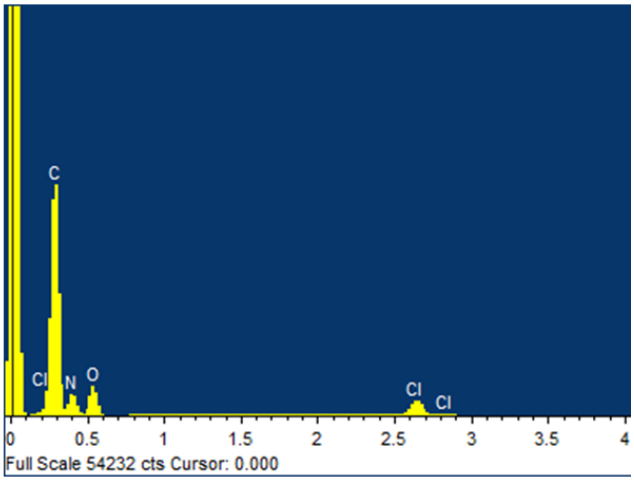

Fig. S12: EDAX analysis of iCOF -2

Section S4

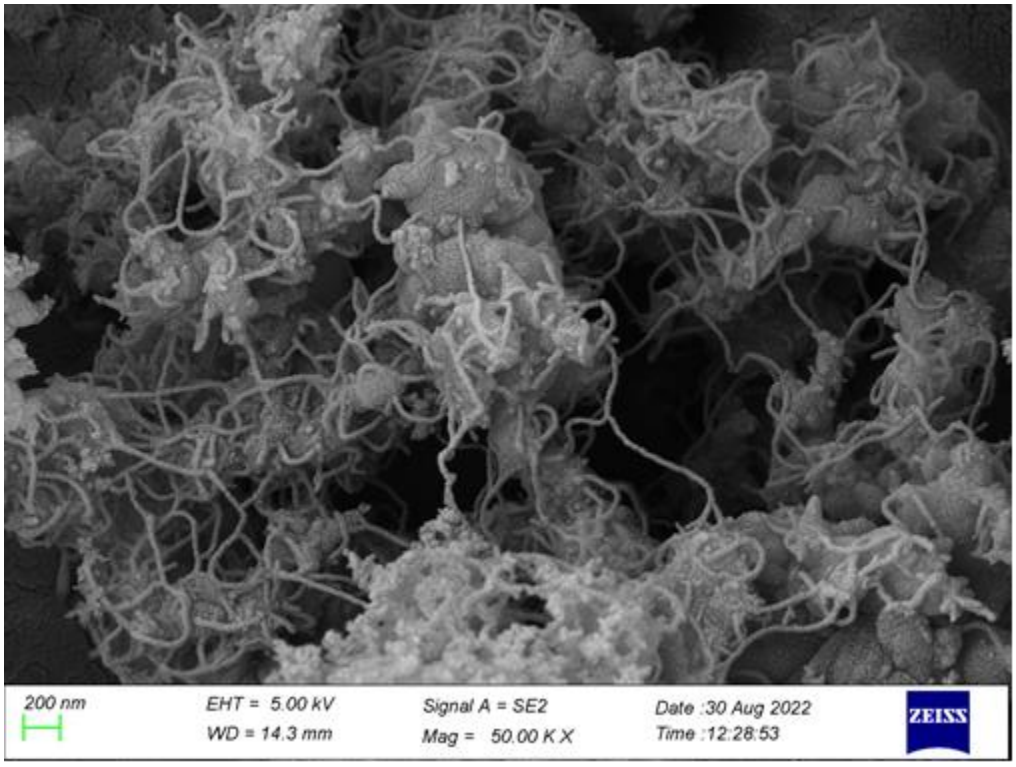

Fig. S13: FE-SEM image of NaOH treated iCOF-2

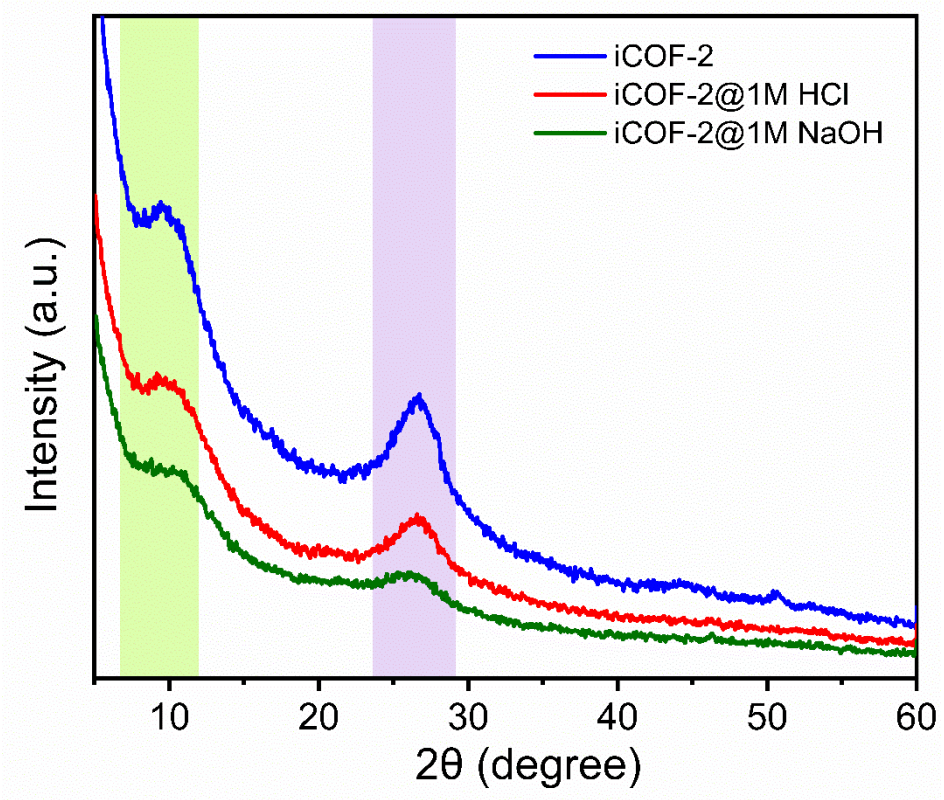

Fig. S14: P-XRD plots of pristine iCOF and acid/base treated iCOF-2

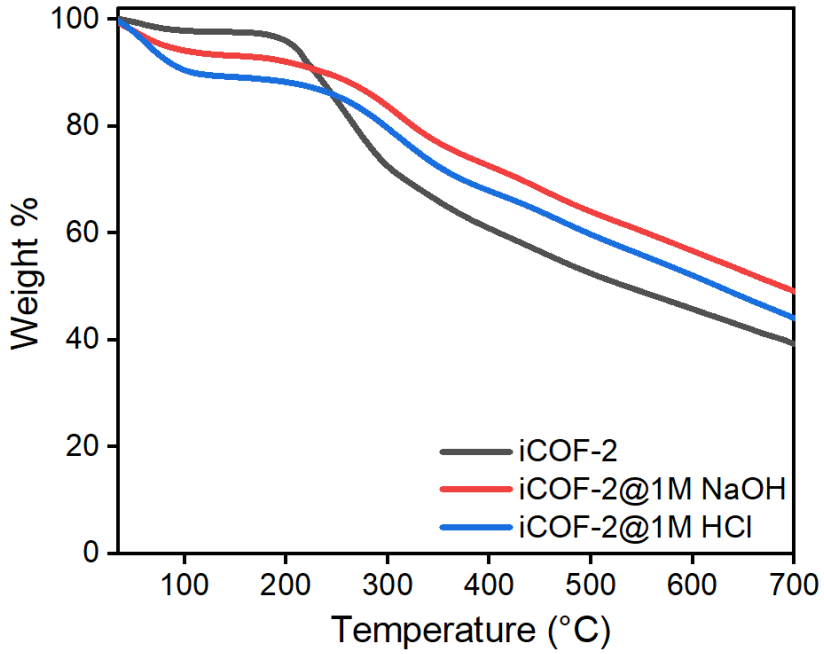

Fig. S15: TGA thermograms of pristine iCOF-2 and acid/base treated iCOF-2

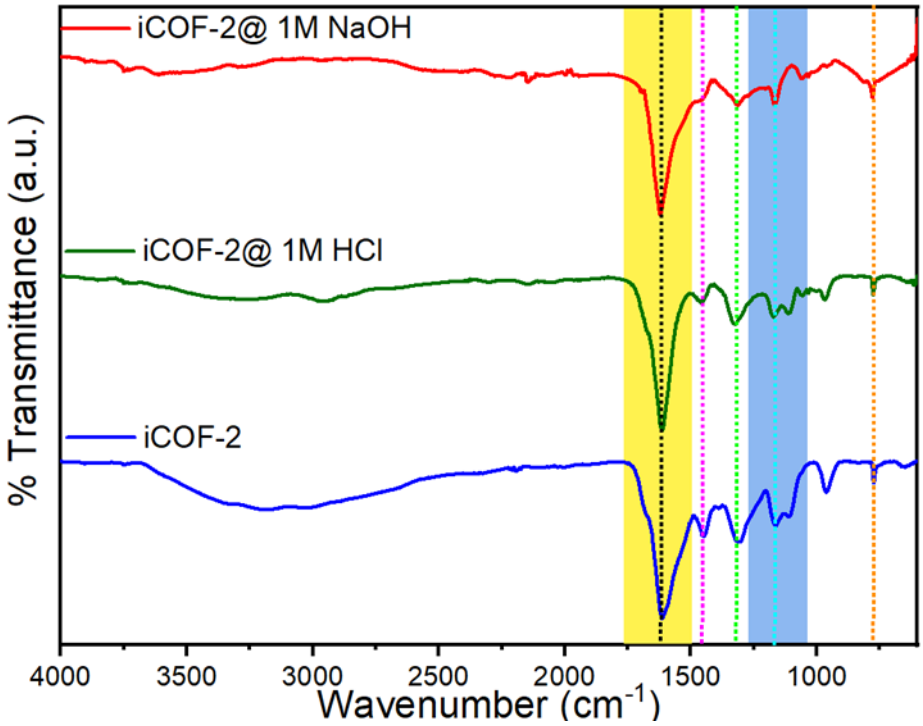

Fig. S16: FT- IR spectra of pristine iCOF and acid/base treated iCOF-2

Section S5

Methods:

Capture studies: iCOF-2 was used to capture various anionic pollutants from respective aqueous solution. Solutions of varying concentration of MnO_4^-, ReO_4^-, I_3^-, CrO_4^{2-}, $Cr_2O_7^{2-}$, and diclofenac were prepared for both kinetic studies and sorption capacity studies.

Kinetic studies: The time-dependent studies for the removal of different anions from water were conducted using UV-visible spectroscopy. A stock solution of the anion to be captured was first prepared, followed by dilution of the stock solution to a pre-determined concentration. The absorbance for the diluted solution was recorded. Next, a fixed quantity of iCOF-2 was added to a specific volume of solution of known concentration with steady stirring. UV-visible spectrum of the supernatant liquid was recorded after diluting it to the same concentration at which the absorbance of other solutions were recorded. From the obtained data, the % removal of the anionic pollutants was calculated using equation (1)

$$\%\ \text{removal} = \frac{C_0 - C_t}{C_0} \times 100\% \quad \text{.....(1)}$$

Where C_0 (mM) is the initial concentration of the anionic pollutants and C_t (mM) is the pollutant concentration at time t. Subsequently, the data was fitted with the non-linear pseudo-second order equations equation (2) for kinetics

$$Q_t = \frac{K_2 Q_e^2 t}{1 + K Q_e t} \quad \text{..... (2)}$$

where Q_t (mg/g) and Q_e (mg/g) are the amounts of sorbate captured by iCOF-2 (sorbent) at different time intervals (t) and at equilibrium respectively. Herein, t represents the time in minutes, K_2 (g mg^{-1} min^{-1}) are the rate constants for pseudo first-order and pseudo-second order reactions respectively.

***K*d calculation formula**

$$K_d = \left(\frac{C_o - C_f}{C_f}\right) \times \frac{V}{M} \quad \text{..... (3)}$$

Using the equation 3, the values of all the distribution coefficients were calculated. Here, C_0 (mM) and C_f (mM) indicate the initial and final concentrations, respectively, whereas K_d is the distribution coefficient. Further, M represents the mass of the sorbent (g), and V denotes the volume of the solution (mL).

Adsorption isotherm experiment: In this experiment, 5 mg of the adsorbent was added to 5 mL of stock solution of a given ion with different concentrations. The mixture was stirred at a constant speed of 550 rpm at room temperature for 12 hours. Subsequently, the adsorbent was filtered off with syringe filter (0.22 µm), and the concentration of remaining (uncaptured) ions in the solution were measured by recording a UV−vis spectrum. The results obtained from these experiments were fitted with following equation (4) and (5) respectively,

Langmuir Model,

$$Q_e = \frac{Q_m K_L C_e}{1 + K_L C_e} \quad \text{..... (4)}$$

Where, C_e (mg L^{-1}) and Q_e (mg g^{-1}) are the concentration of analyte at equilibrium and amount of analyte adsorbed at equilibrium respectively. Q_m (mg g^{-1}) is the maximum amount of analyte per mass of adsorbent to form a complete monolayer. K_L (mg L^{-1}) is a constant related to the affinity of the binding sites.

Freundlich Model,

$$Q_e = K_F C_e^{1/n} \text{..... (5)}$$

Where, K_f and 1/n are the Freundlich model constant, indicating capacity and intensity of adsorption respectively.

Iodine sorption experiments in vapor phase:

In this experiment, 20 mg of iCOF-2 was taken in a sealed chamber and exposed to iodine vapor for over 48 hours at 75 °C and ambient pressure. In this experiment, initially the polymer sample was activated and placed in a small open vial (5 ml capacity). Next, this small vial was placed inside another larger vial (15 ml capacity) to avoid the direct contamination. Then, the larger vial (15 ml capacity) was further kept inside a glass chamber with iodine granules present at the bottom. Subsequently, glass chamber was sealed and kept in an oven at 75 °C. Periodically, the weight of the smallest vial (5 ml capacity and containing iCOF-2) was recorded. A gradual but significant colour change was observed in iCOF-2 with the onset of iodine adsorption till the experiment ended. The iodine uptake capacities were calculated using the equation (6).

$$\alpha = \frac{m_2 - m_1}{m_1} \text{ ..... (6)}$$

where α is the iodine uptake capacity in g/g and m_1, m_2 are the weight of the vial containing iCOF-2 before and after the start of the iodine vapor capture experiment.

Real-time experiments: 0.25 mM stock solutions of the pollutants were prepared using water collected for tap, tannery, pond, lake, river and sea. To 5 ml of these solutions, 10 mg of iCOF-2 was added and the mixture was stirred for 3 hours. The adsorbent (iCOF-2) was then filtered out and the filtrate was analysed using UV-vis spectroscopy. The uptake capacities were calculated from the values of the initial and final absorbance of the filtrate.

Selectivity studies: 5 mg of iCOF-2 was introduced to a binary solution consisting of 5 mL of 0.1 mM of the target anionic pollutant (MnO_4^-, ReO_4^-, CrO_4^{2-}, $Cr_2O_7^{2-}$, MnO_4^-, I_3^-, diclofenac sodium) and 5 ml of 0.1 mM solutions containing various interfering ions (Cl^-, Br^-, NO_3^- and SO_4^{2-}). The mixture was then filtered and the filtrate was analysed using UV-vis spectroscopy. For 1:20 ratio of interfering ions, the analyte concentration changes respectively.

Regeneration studies: Post anion capture experiments, iCOF-2 loaded with pollutants were regenerated by treating such samples with a dilute solution of NaOH, dilute HCl or 1:1 mixture of MeOH and saturated brine in sequence.

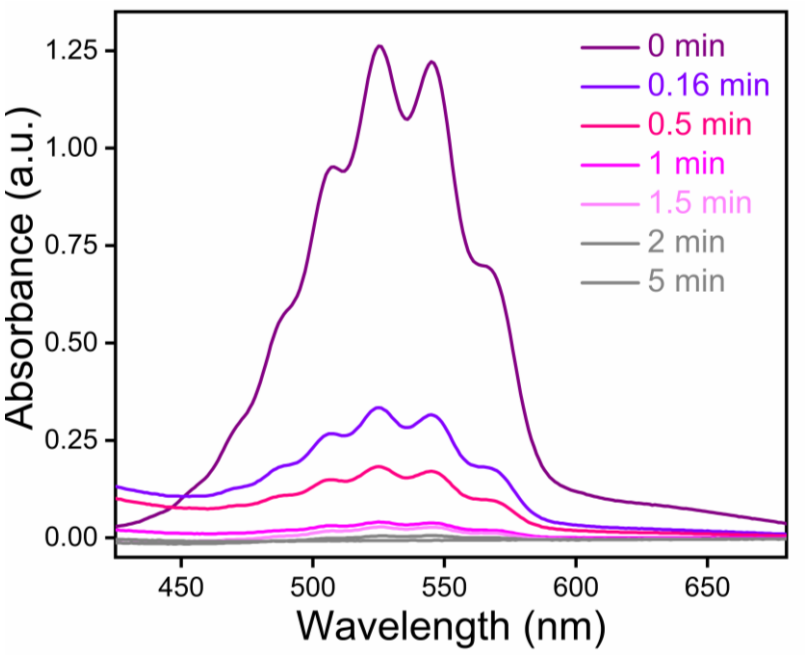

Fig. S17a: Time dependent UV-vis spectra of MnO_4^-

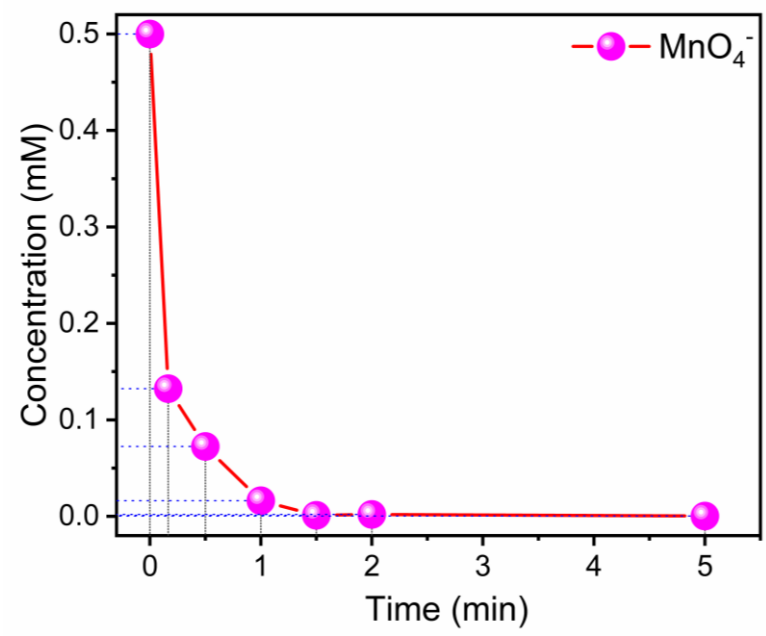

Fig. S17b: Concentration change of MnO_4^- with time.

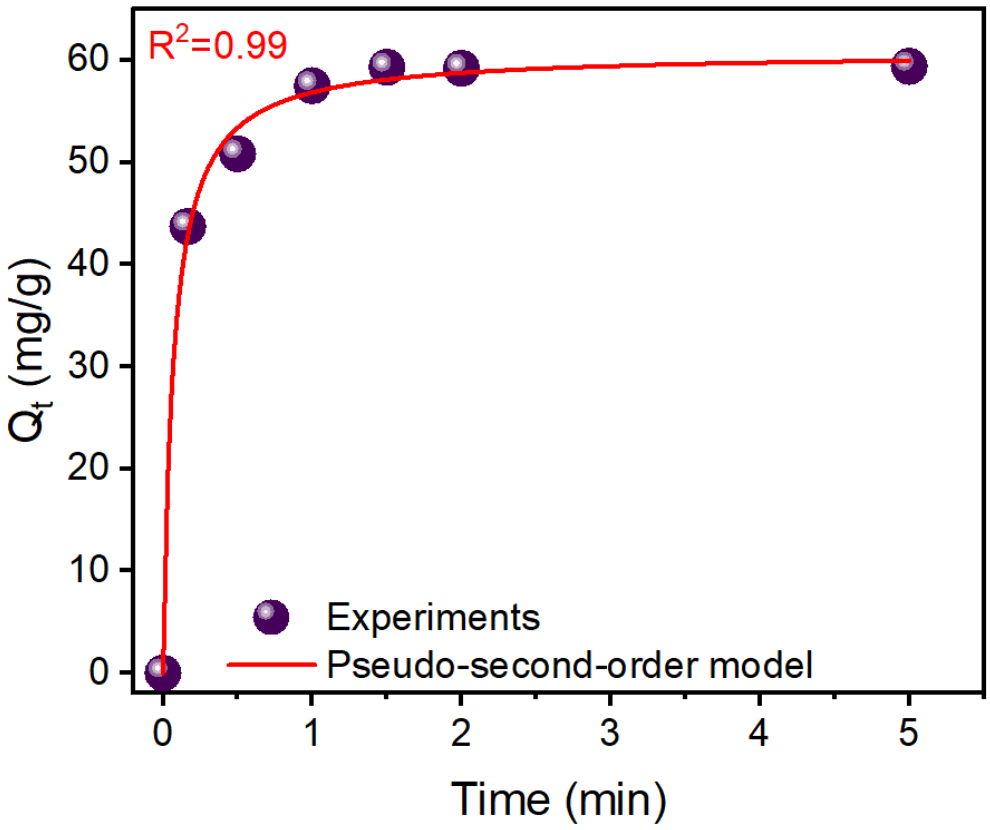

Fig. S17c: Pseudo second order kinetic rate model fitting for MnO_4^- capture.

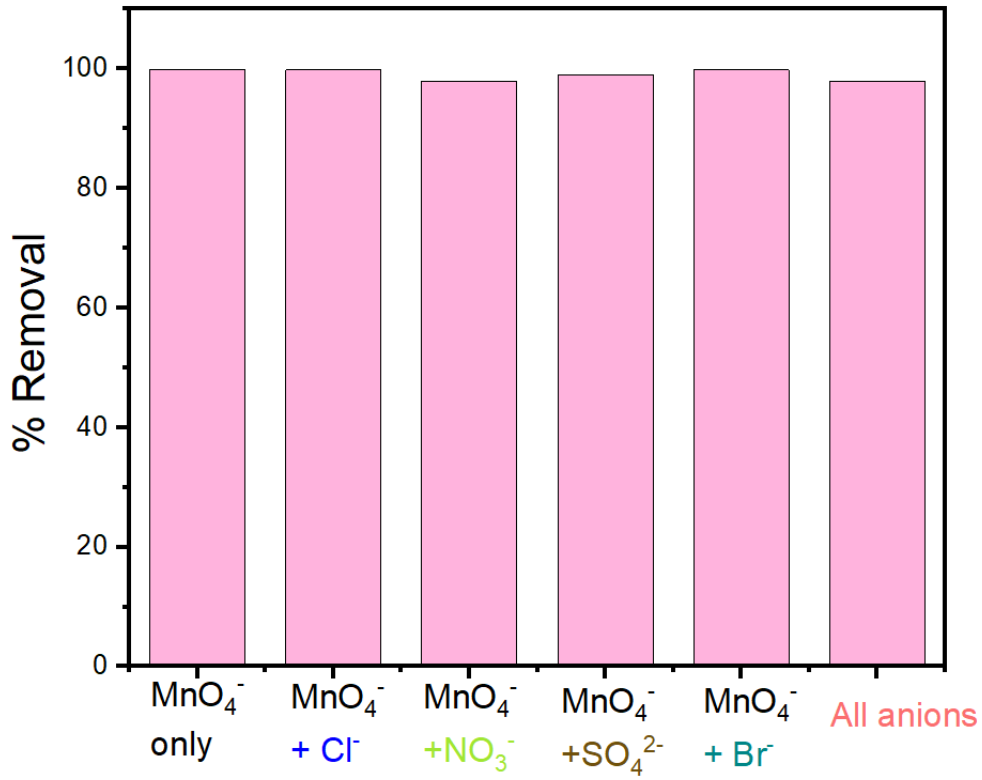

Fig. S17d: MnO_4^- removal with 1:1 ratio of other interfering anions

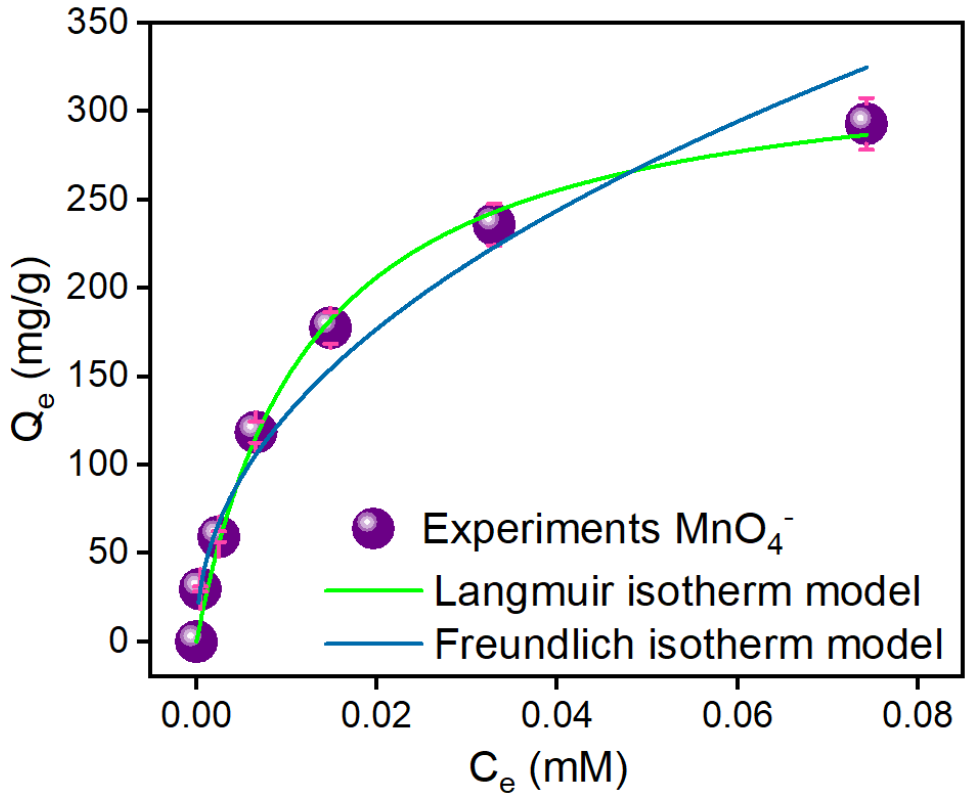

Fig. S17e: Isotherm fitting for MnO_4^- capture

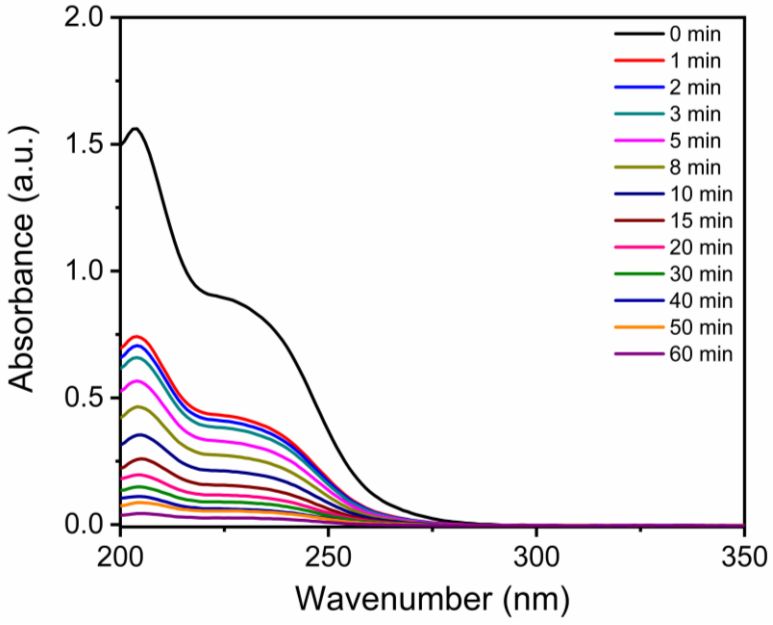

Fig. S18a: Time dependent UV-vis spectra of ReO_4^- capture experiment

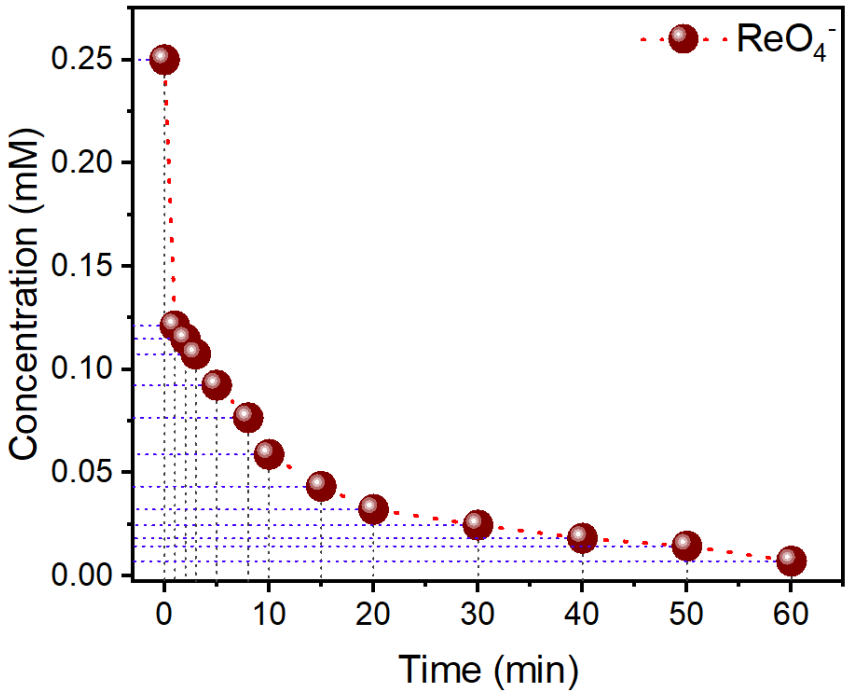

Fig. S18b: Decrease in the concentration of ReO_4^- with time

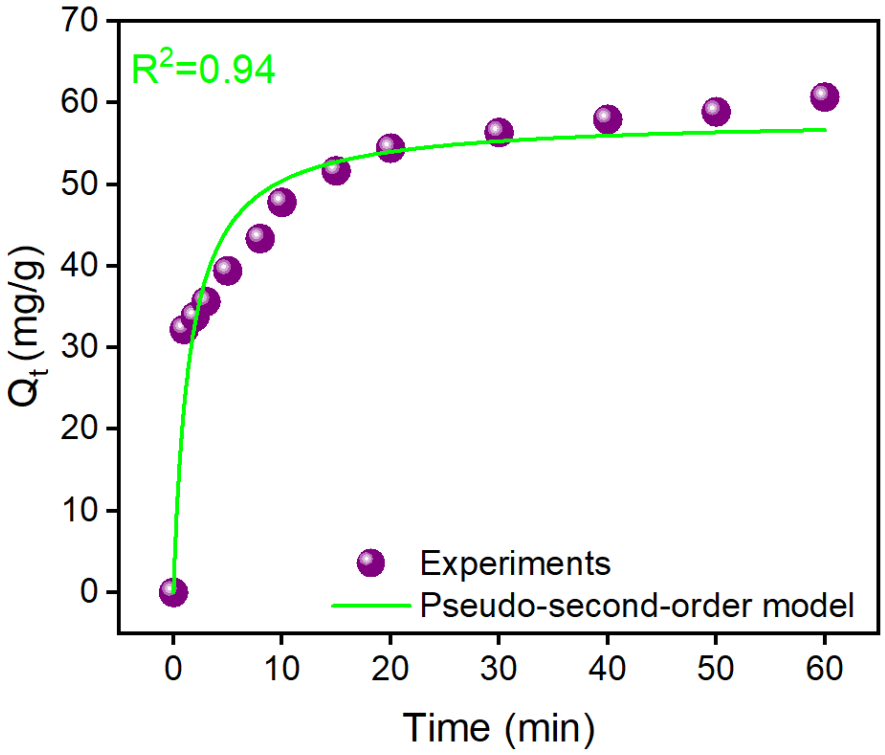

Fig. S18c: Pseudo second order kinetic rate model fitting of ReO_4^- capture data.

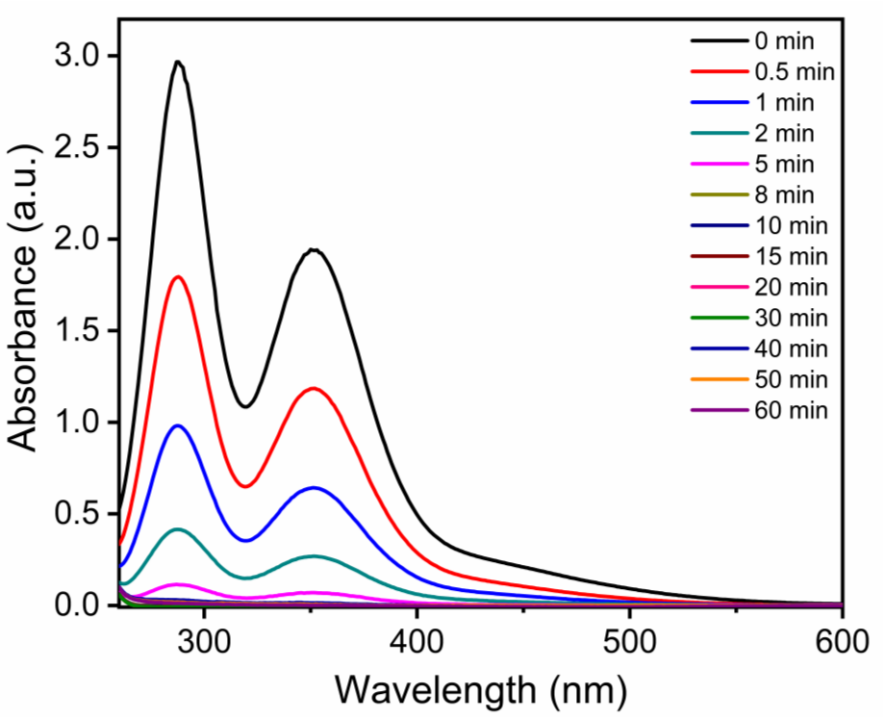

Fig. S19a: Time dependent UV-vis spectra of I_3^- capture from its aqueous solution

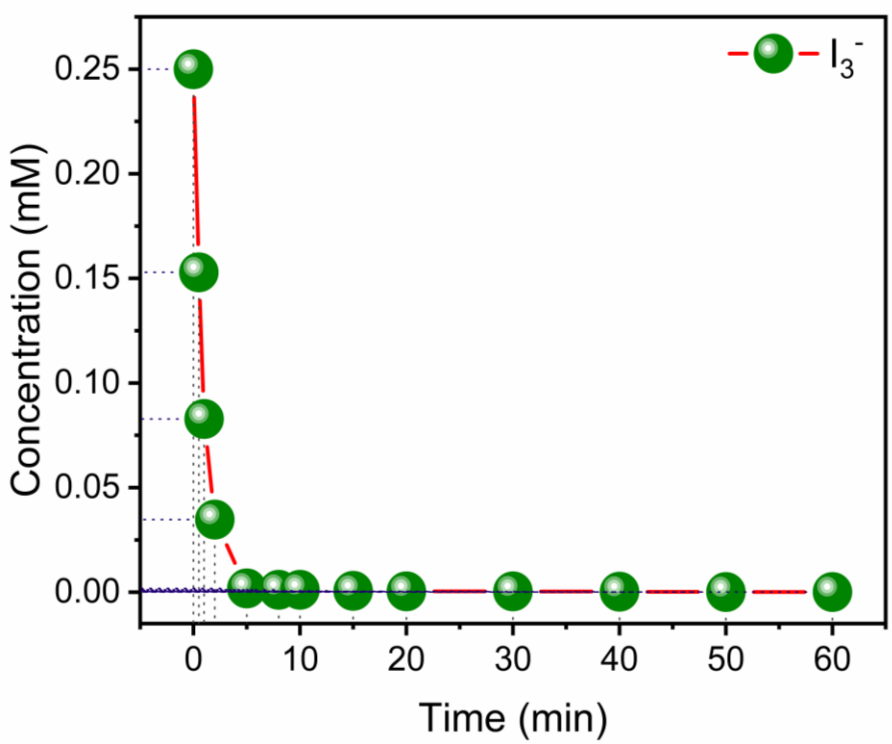

Fig. S19b: Change in the concentration of I_3^- with time

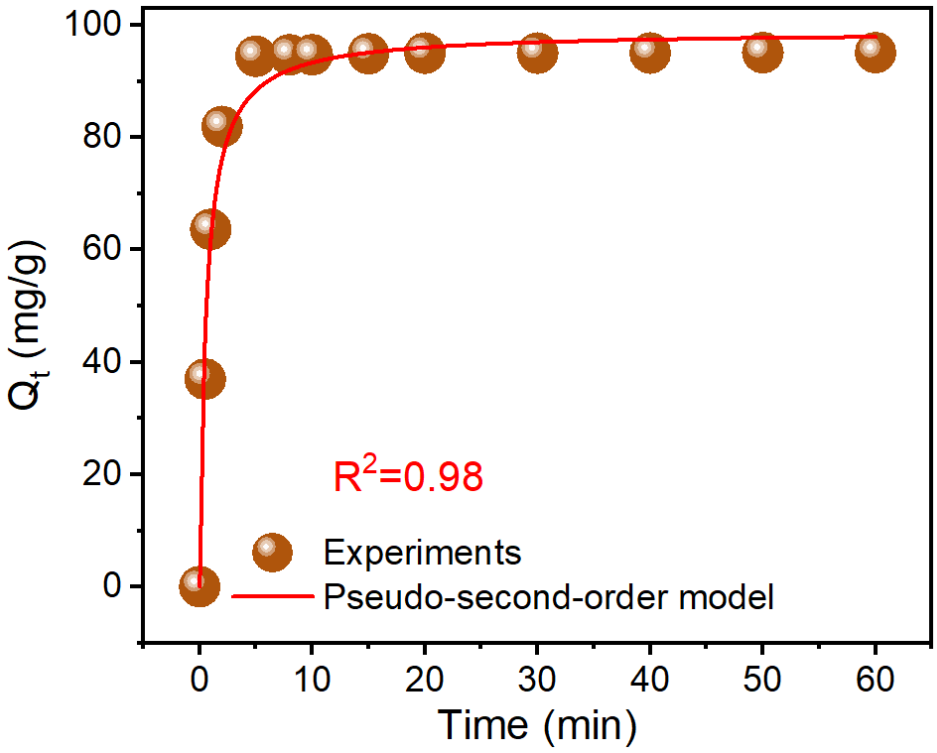

Fig. S19c: Pseudo second order kinetic rate model fitting of I_3^- capture data

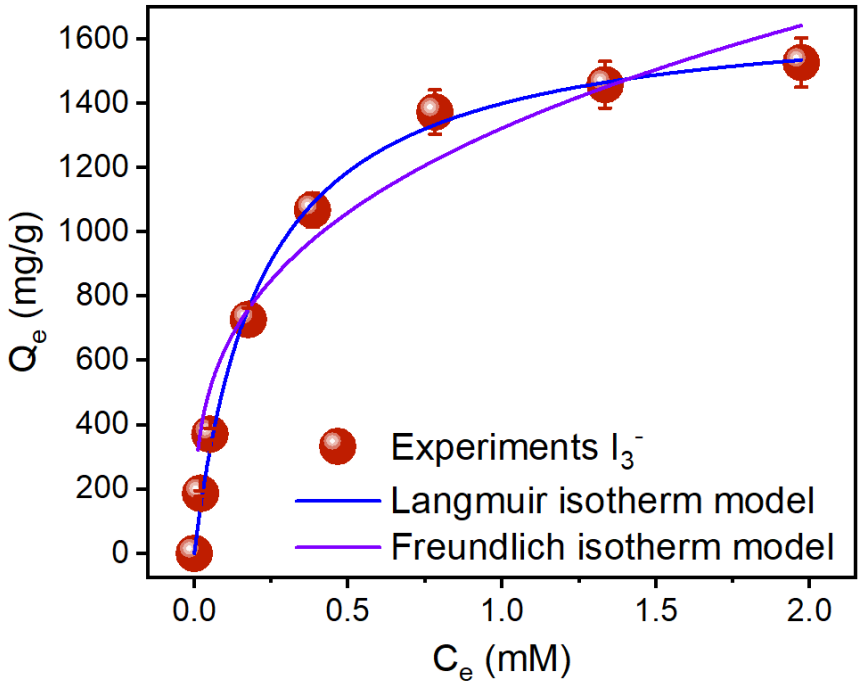

Fig. S19d: Isotherm fitting for I_3^- capture

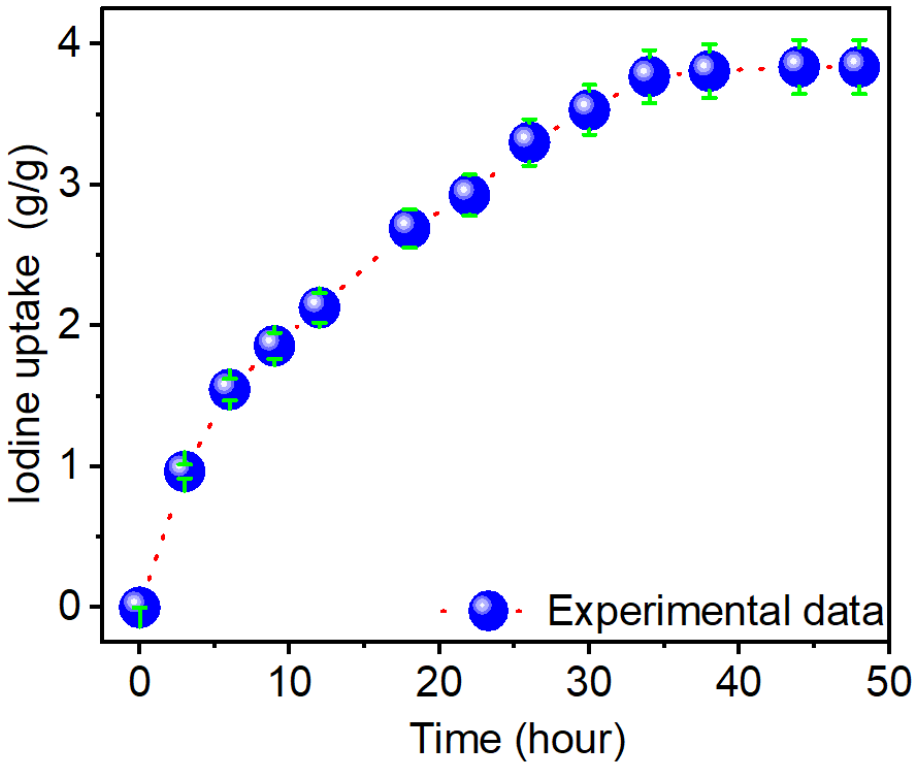

Fig. S19e: Gravimetric iodine capture by iCOF-2

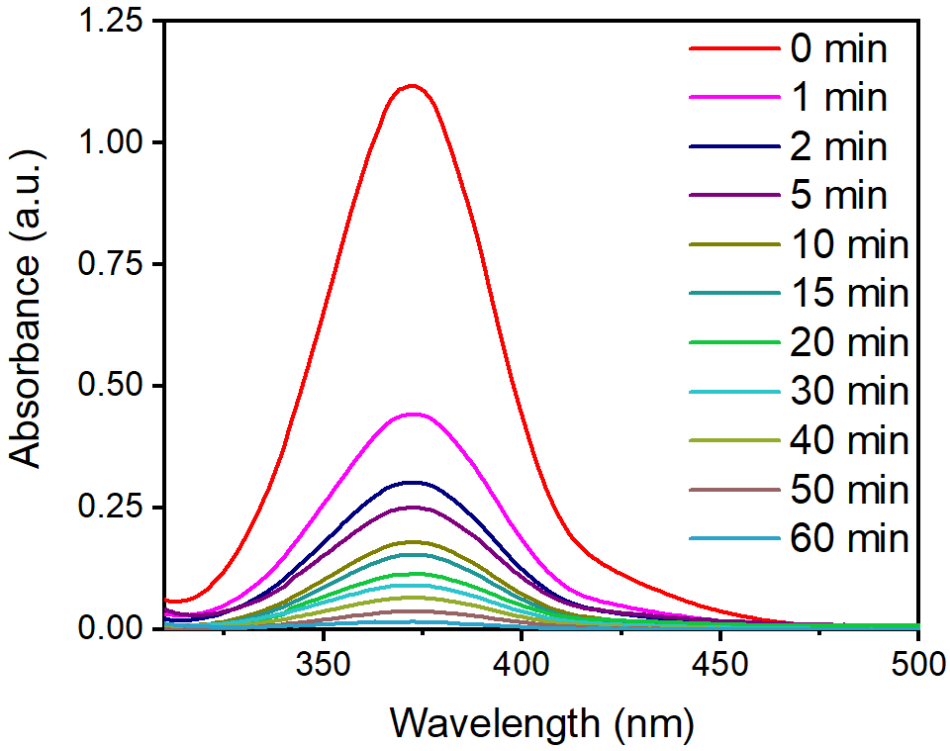

Fig. S20a: Time dependent capture of CrO_4^{2-} using UV-vis spectroscopy

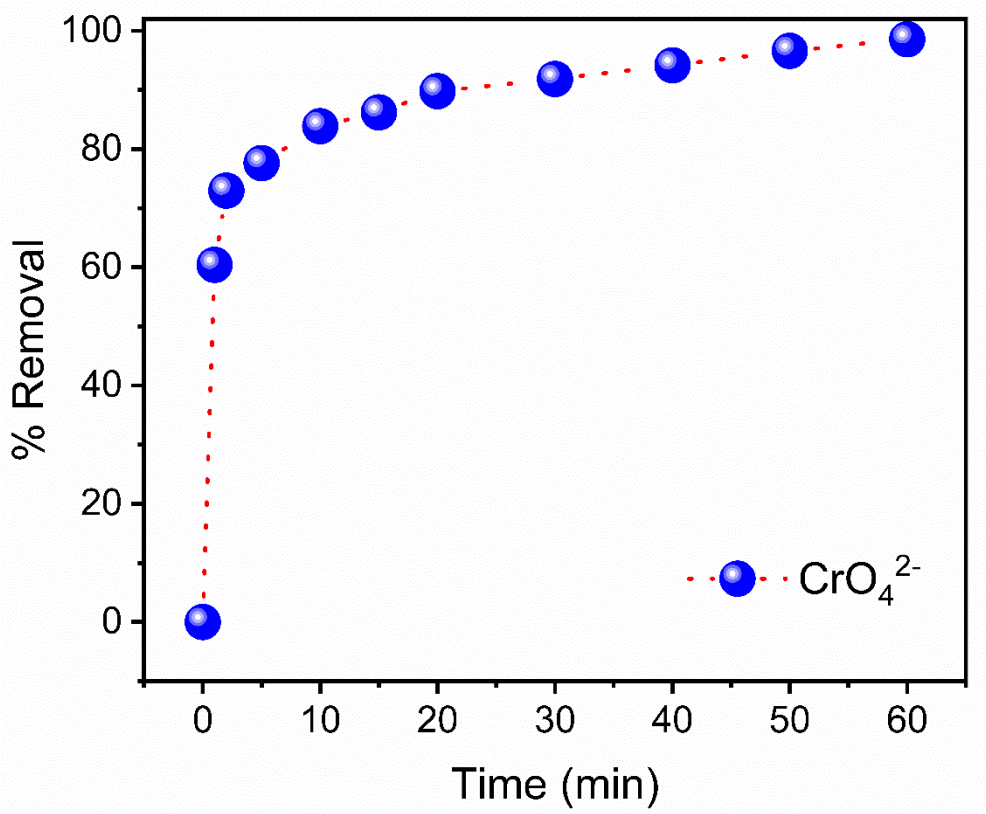

Fig. S20b: Time dependent percentage removal of CrO_4^{2-}

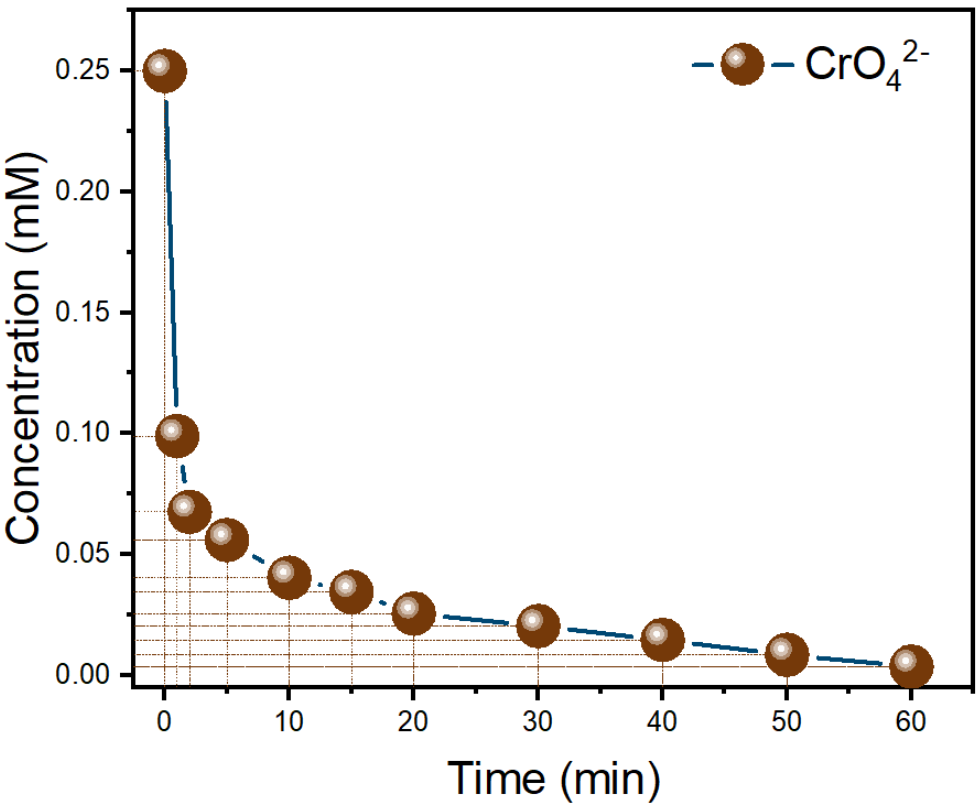

Fig. S20c: Change in CrO_4^{2-} concentration with time

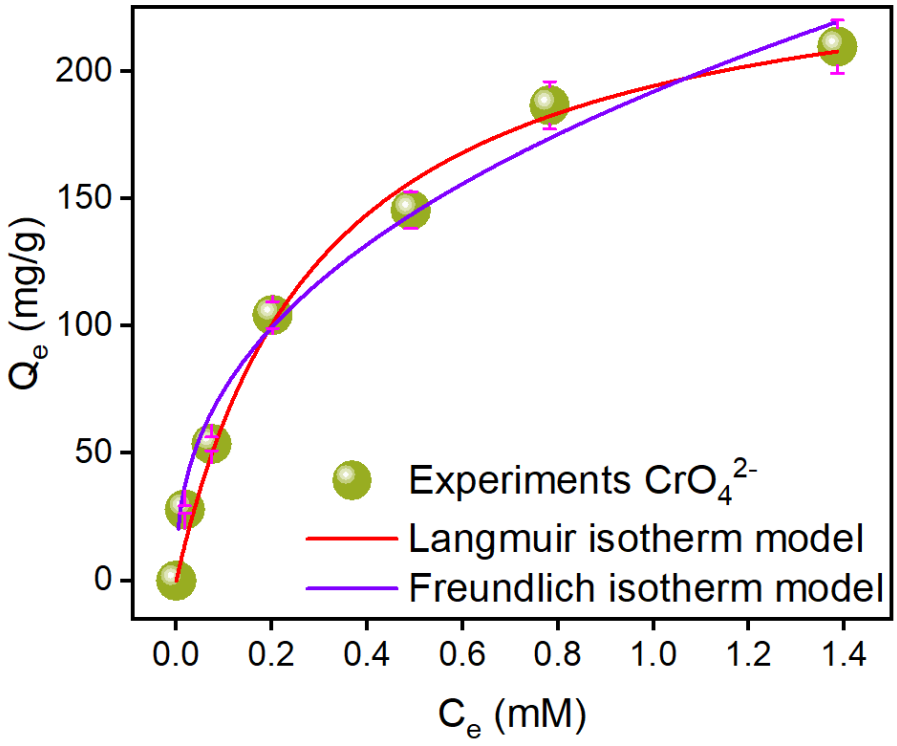

Fig. S20d: Isotherm fitting for CrO_4^{2-} capture

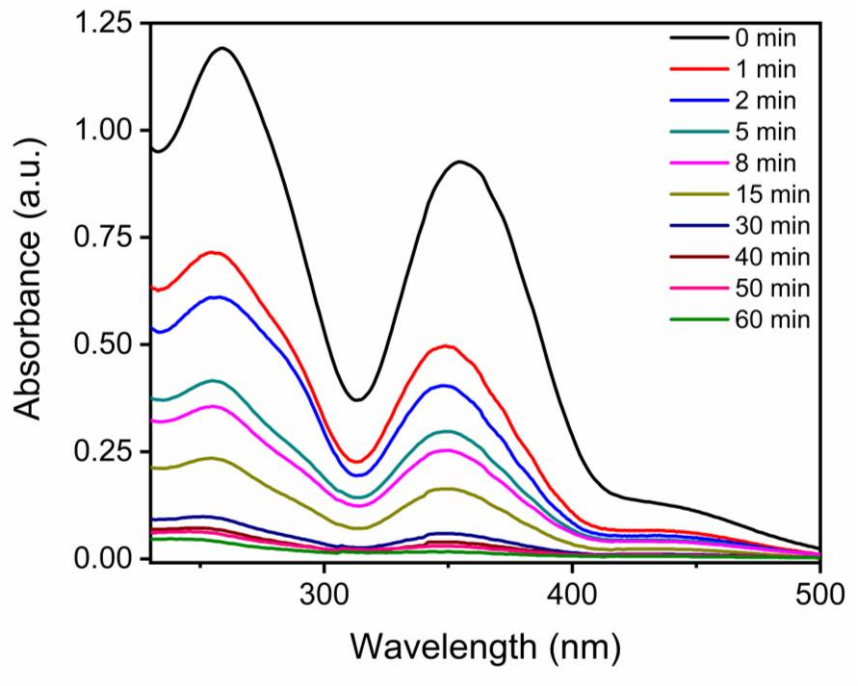

Fig. S21a: Time dependent UV-vis spectra of $Cr_2O_7^{2-}$ capture from its aqueous solution

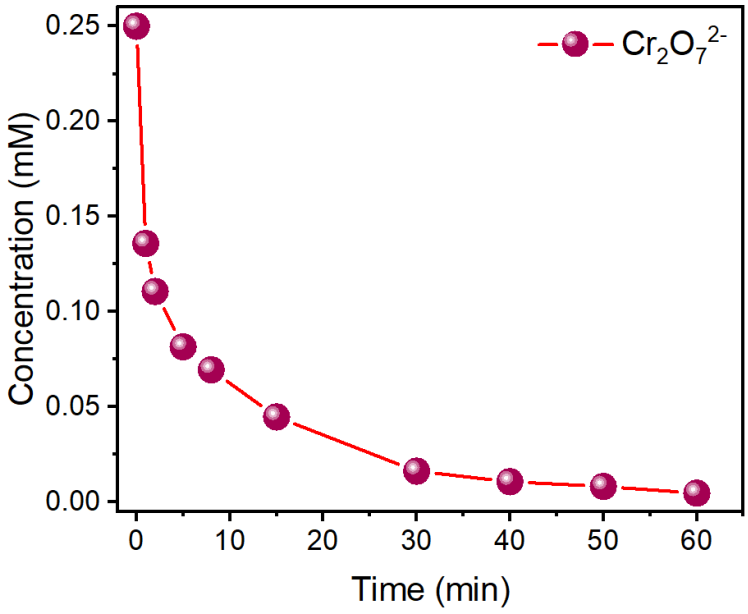

Fig. S21b: Change in the concentration of $Cr_2O_7^{2-}$ with time

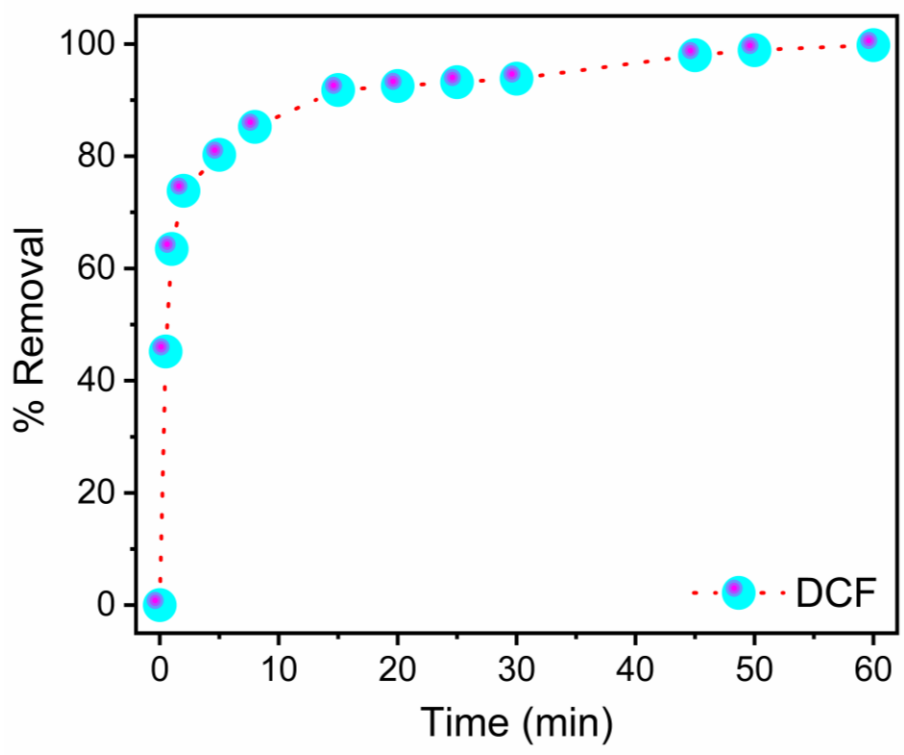

Fig. S22a: % removal vs time of DCF

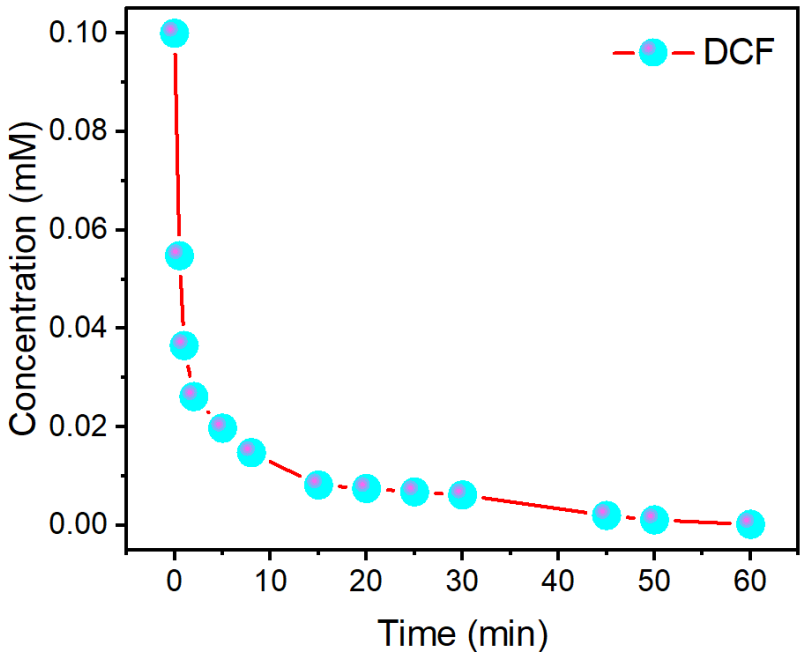

Fig. S22b: Decrease in the concentration of DCF with time

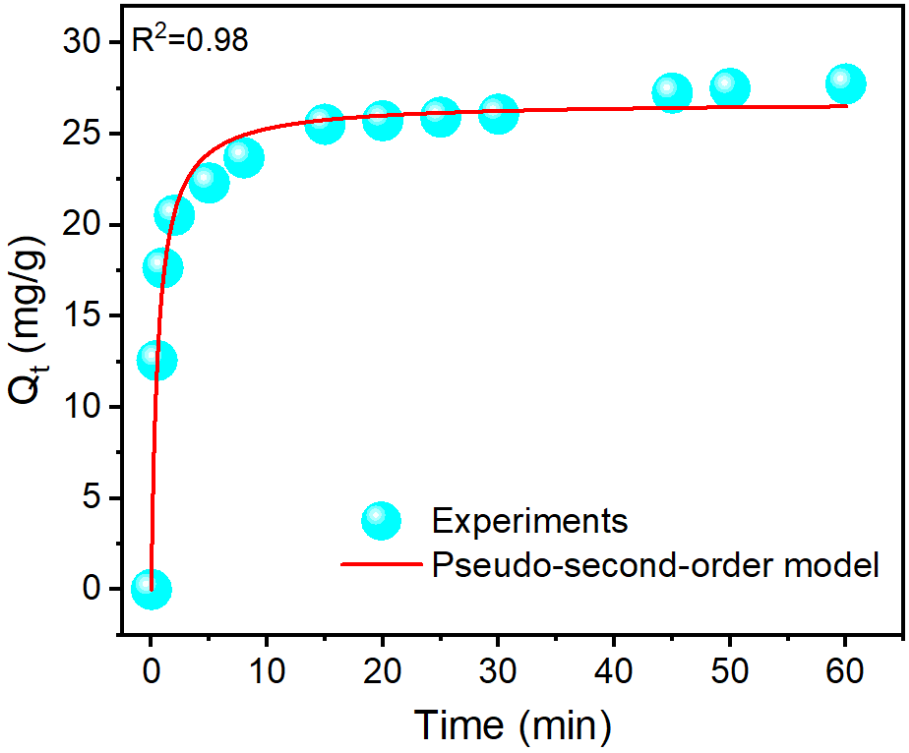

Fig. S22c: Pseudo second order kinetic rate model fitting of DCF^{-} capture

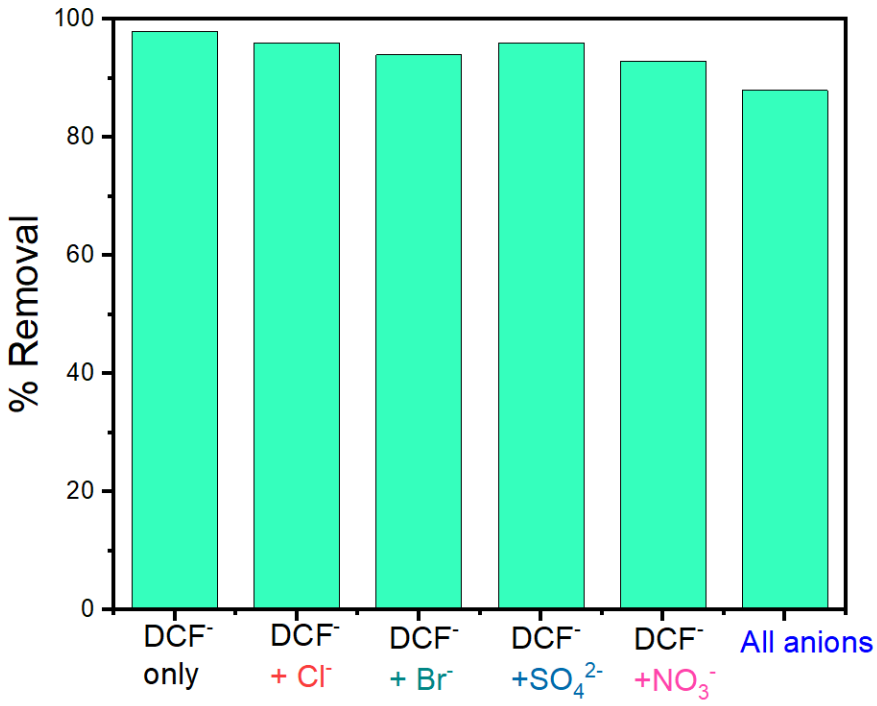

Fig. S22d: DCF⁻ removal in presence of other interfering anions

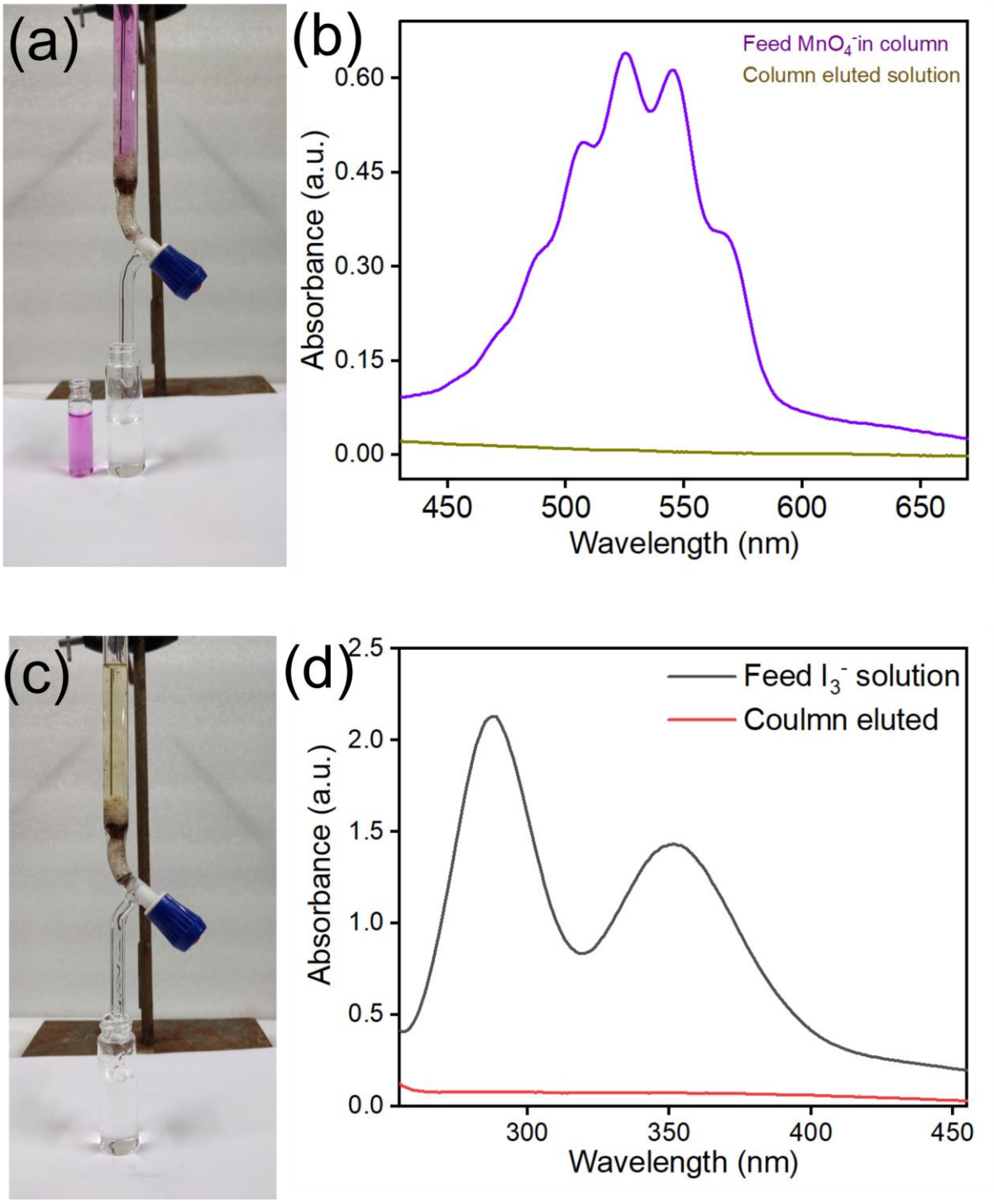

Fig. S23: (a) Column based capture of MnO_4^- (b) UV-vis spectra of column eluted solution MnO_4^- (c) Column based capture of I_3^- (d) UV-vis spectra of column eluted solution I_3^-

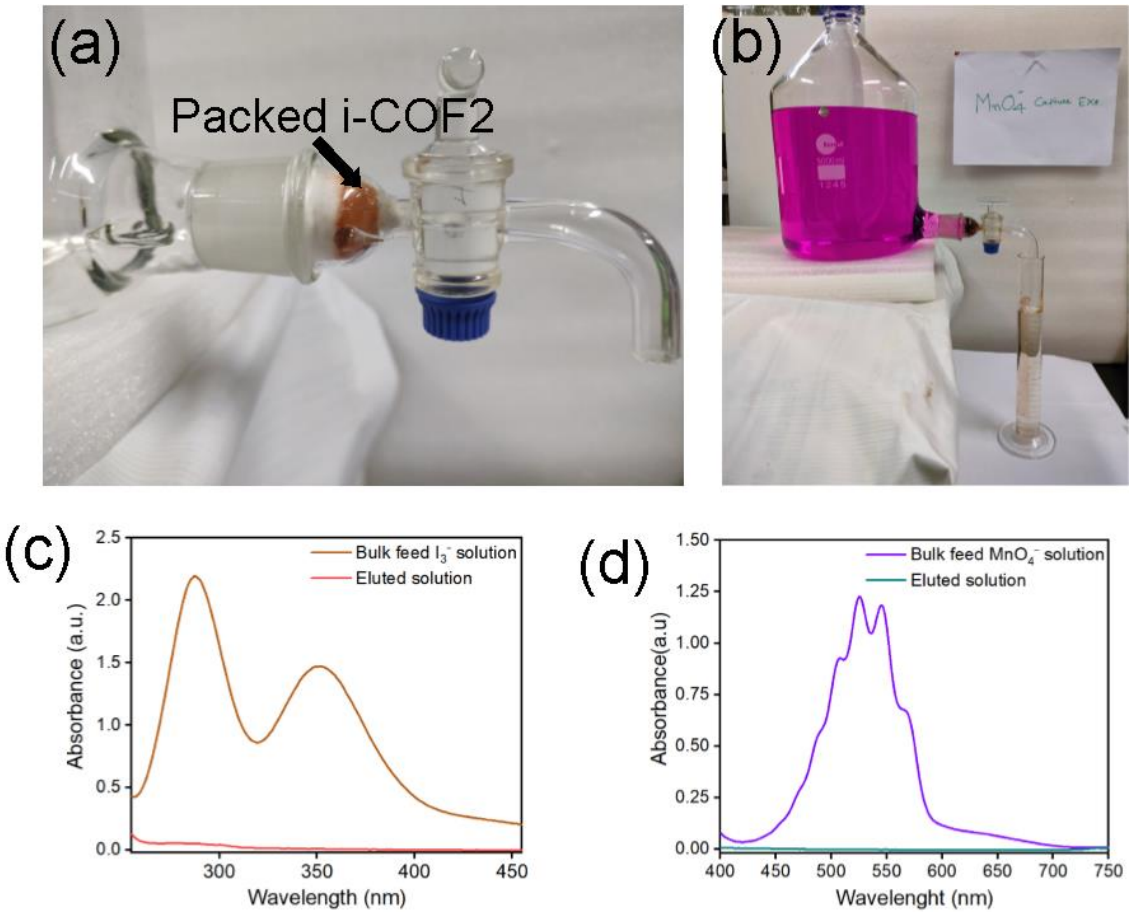

Fig. S24: (a) Packing of i-COF-2 (b) Bulk purification of MnO_4^- contaminated water with a MnO_4^- as a model pollutant (c) UV-vis spectra of eluted solution I_3^- (d) UV-vis spectra solution of MnO_4^-

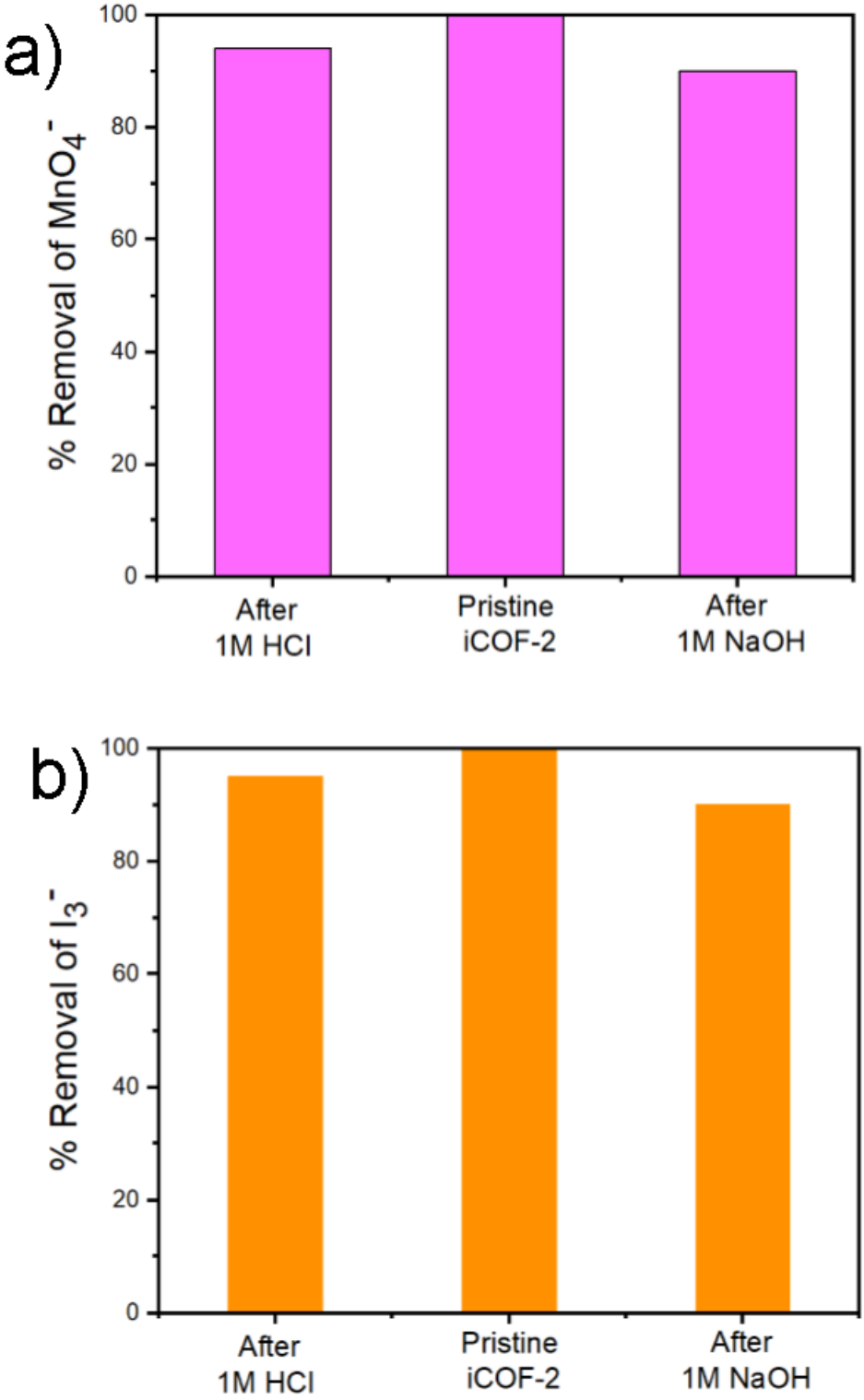

Fig. S25: Removal experiments after acid/base treatment of pristine iCOF-2

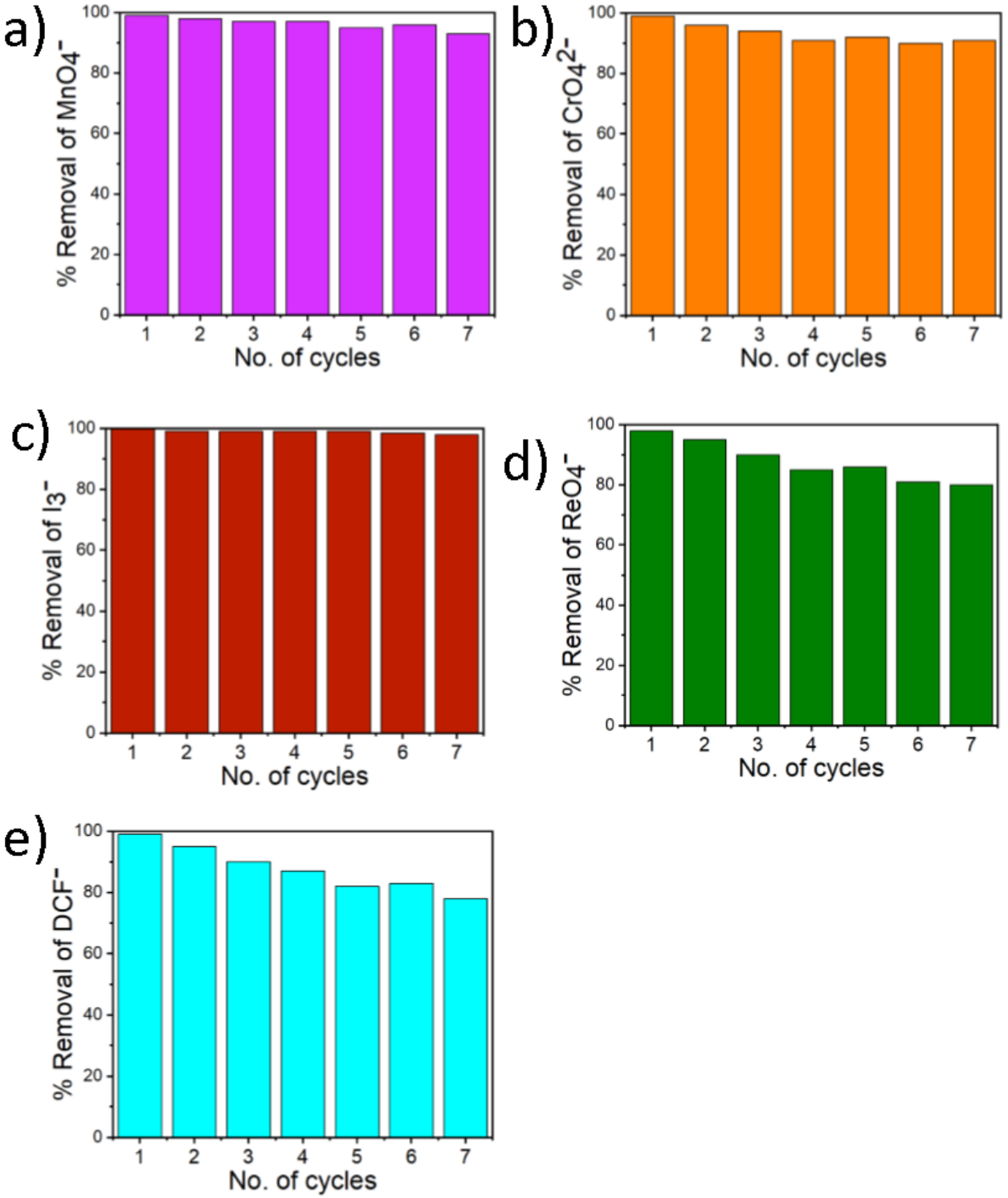

Fig. S26: Reusability of iCOF-2 for different anionic pollutants.

Section S6

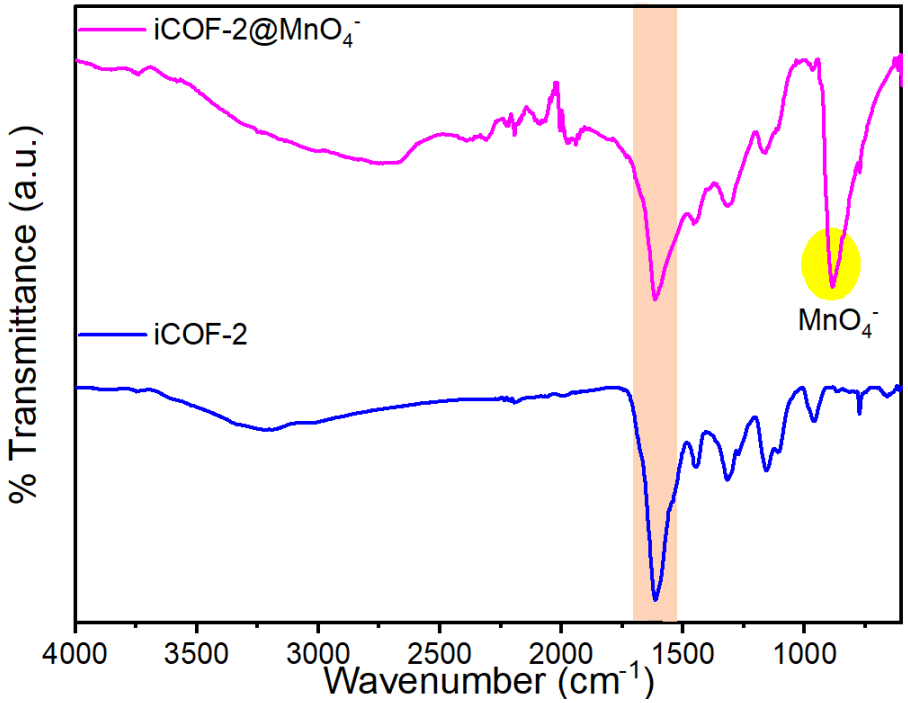

Fig. S27a: Post-capture FT-IR spectra of iCOF-2@MnO_4^- compared with pristine iCOF-2

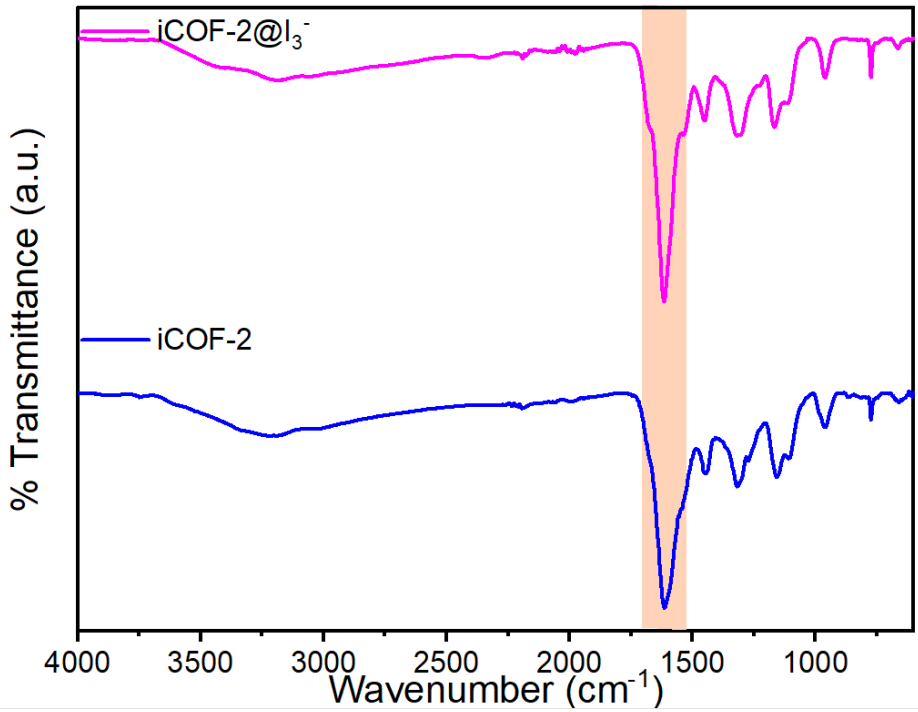

Fig. S27b: Post-capture FT-IR spectra iCOF-2@ of I_3^- and pristine iCOF-2.

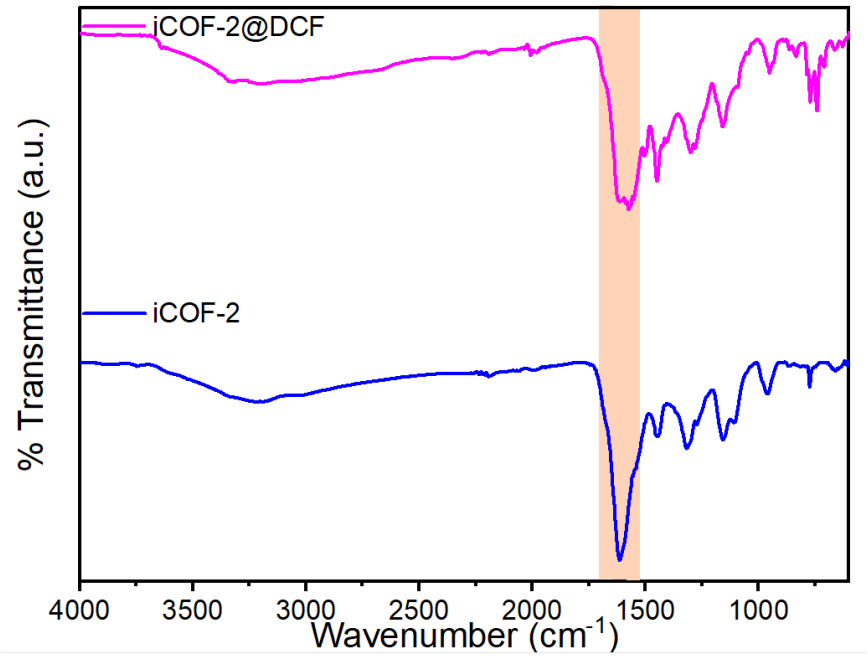

Fig. S27c: Post-capture FT-IR spectra of iCOF-2@DCF⁻ and pristine iCOF-2.

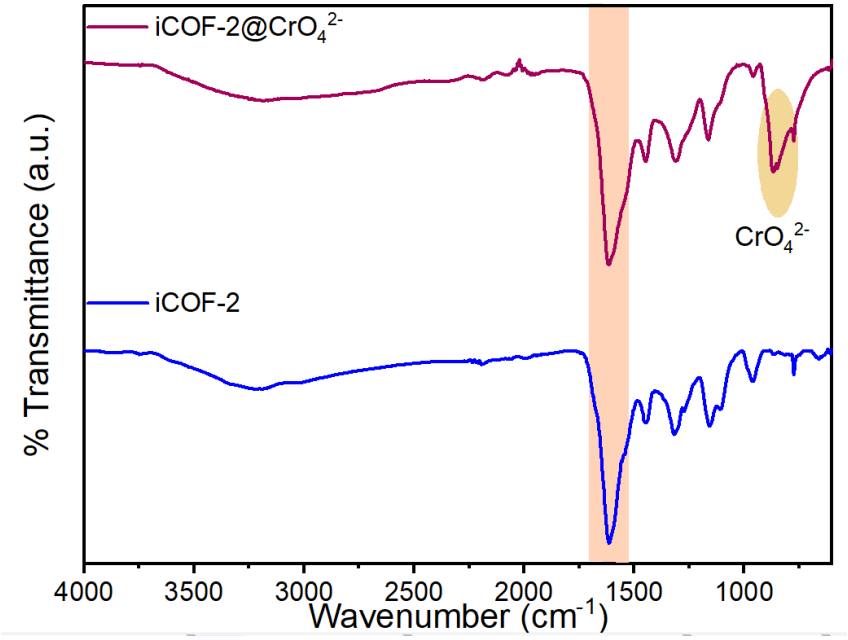

Fig. S27d: Post-capture FT-IR spectra of CrO_4^{2-}@iCOF-2 and pristine iCOF-2.

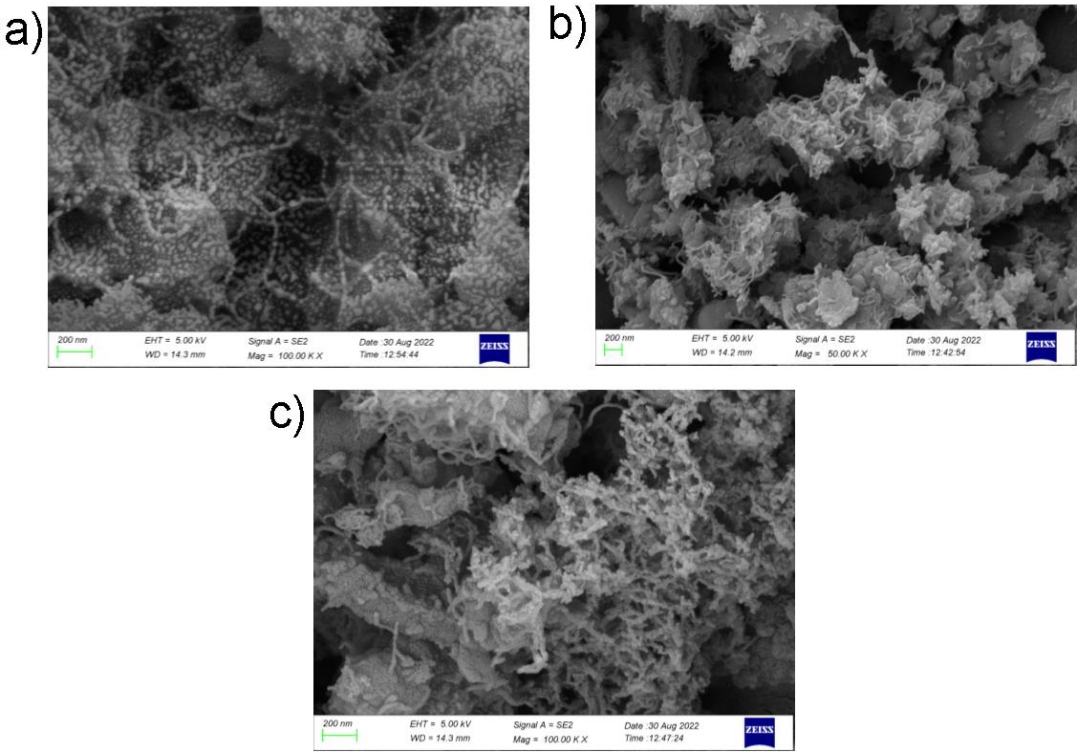

Fig. S28: Post capture FE-SEM images of (a) I_3^-@iCOF-2 (b) CrO_4^{2-}@ iCOF-2, (c) ReO_4^- @iCOF-2

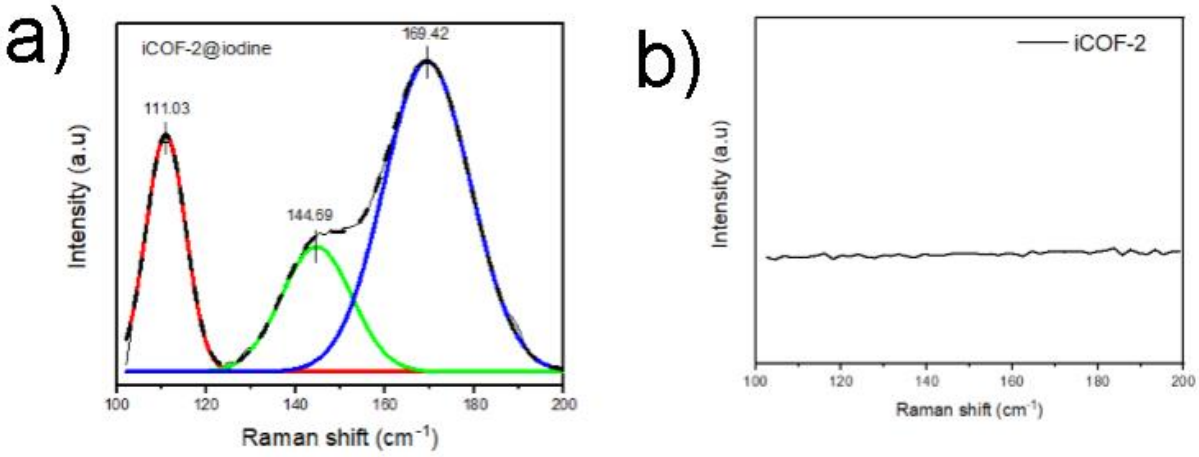

Fig. S29: Raman spectrum of (a) iodine captured iCOF-2 (b) Pristine iCOF-2

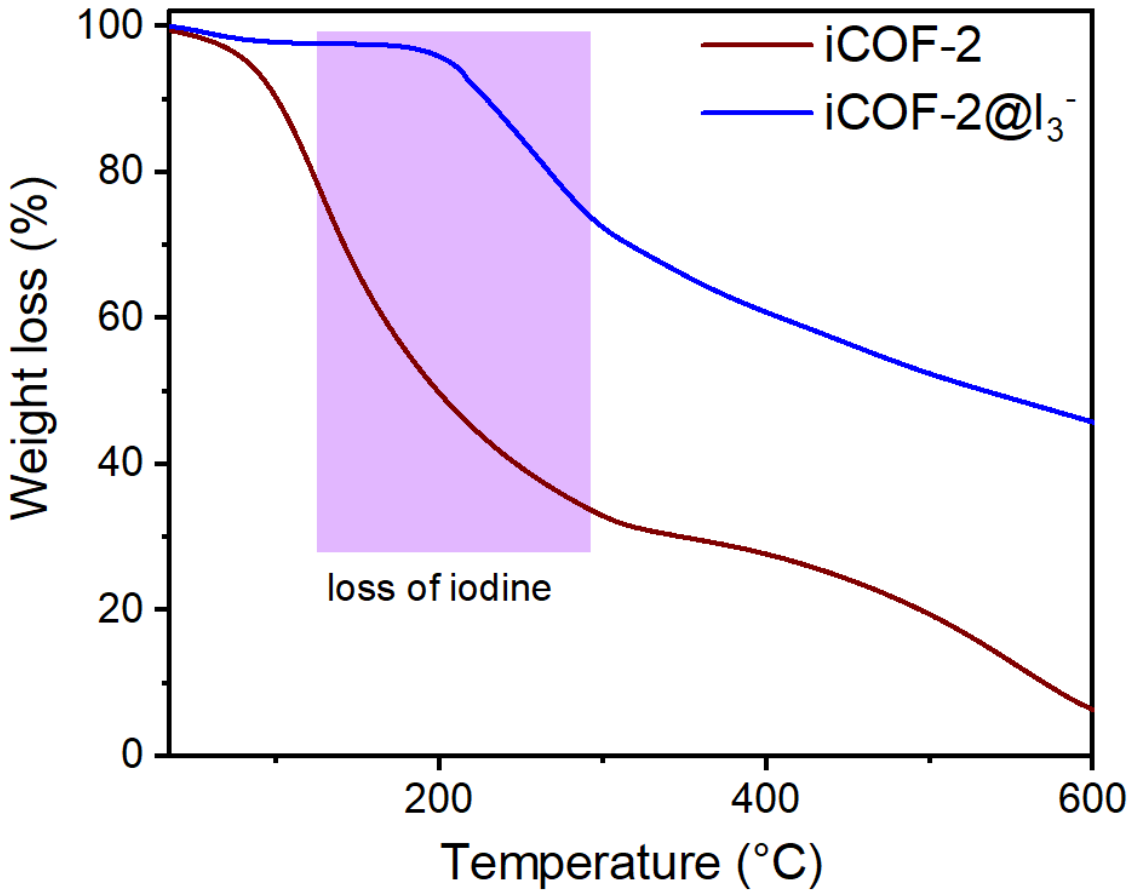

Fig. S30: TGA thermogram of iCOF-2@ I_3^- and pristine iCOF-2.

Element	Weight%	Atomic%
C K	57.79	69.24
N K	1.77	1.82
O K	28.77	25.88
Cl K	0.06	0.02
Mn K	11.61	3.04
Totals	100.00	

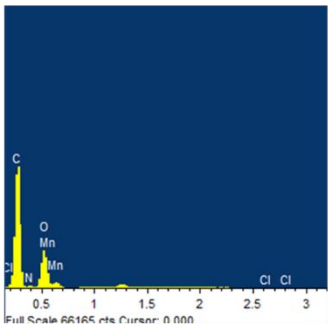

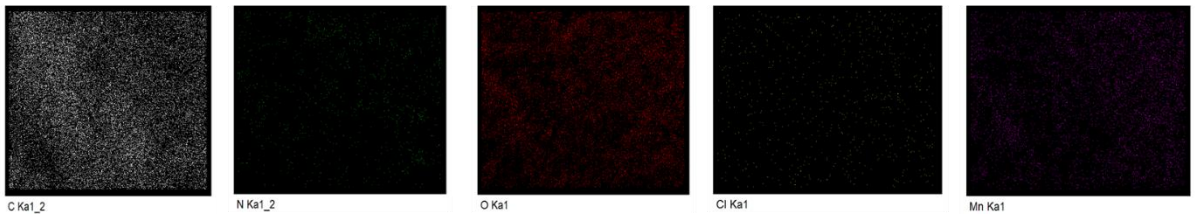

Fig. S31a EDX and elemental mapping analysis of the iCOF-2@MnO_4^-

Element	Weight %	Atomic%
C K	43.88	54.88
N K	25.91	27.78
O K	17.33	16.27
Cl K	0.10	0.04
Re M	12.78	1.03
Totals	100.00	

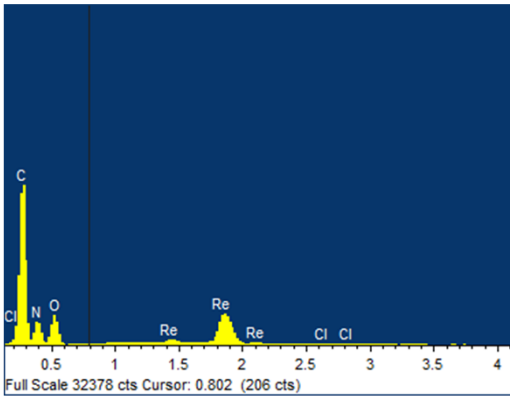

Fig. S31b EDX analysis of the iCOF-2@ReO_4^-

Element	Weight%	Atomic%
C K	39.29	58.70
N K	18.78	24.06
O K	11.29	12.66
Cl K	0.70	0.36
I L	29.93	4.23
Totals	100.00	

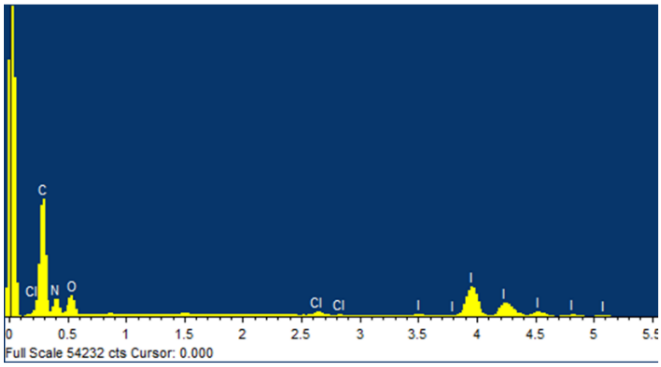

Fig. S31c EDX analysis of the iCOF-2@I_3^-

Element	Weight%	Atomic%
C K	54.12	59.74
N K	26.25	24.84
O K	18.14	15.03
Cl K	0.00	0.00
Cr K	1.50	0.38
Totals	100.00	

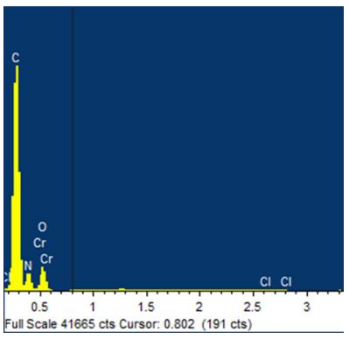

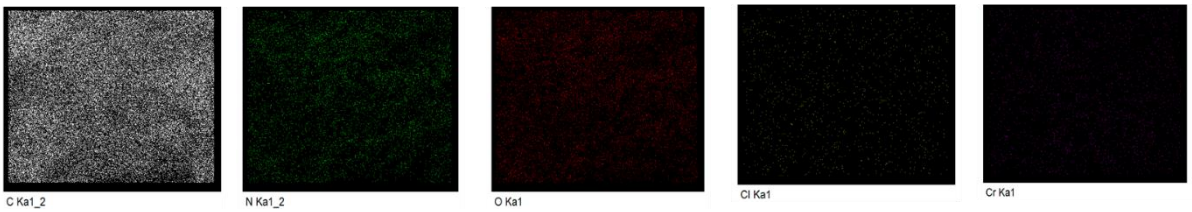

Fig. S31d EDX and elemental mapping analysis of the iCOF-2@ CrO_4^{2-}

Section S7:

Table-S2

Analyte	Name of the Adsorbate	Capacity (mg/g)	Selectivity	Reference
MnO_4^-	**iCOF-2**	**334**	**Cl^-, NO_3^-, Br^-, SO_4^{2-}**	**This work**
ReO_4^-	**iCOF-2**	**325**	**Cl^-, NO_3^-, Br^-, SO_4^{2-}**	**This work**
CrO_4^{2-}	**iCOF-2**	**253**	**Cl^-, NO_3^-, Br^-, SO_4^{2-}**	**This work**
I_3^-	**iCOF-2**	**1705**	**Cl^-, NO_3^-, Br^-, SO_4^{2-}**	**This work**
DCF $^-$	**iCOF-2**	**235**	**Cl^-, NO_3^-, Br^-, SO_4^{2-}**	**This work**
ReO_4^-	3DCOF-g-VBPPh 3Cl	181	**SO_4^{2-}**, NO_3^-, Cl^-, PO_4^{3-}	*Adv. Funct. Mater.* **2022**, *2205222*
ReO_4^-	SCU-102	291	NO_3^-, ClO_4^- SO_4^{2-}, PO_4^{3-}	*Angew.Chem. Int. Ed.* **2019**, *58,4968 –4972*
ReO_4^-	Ag-TPPE	251	NO_3^-, SO_4^{2-}	*Adv. Funct. Mater.* **2022**, 2208148
ReO_4^-	Superphane 2	267	NO_3^-, Cl^-, F^-, HCO_3,ClO_4^- $H_2PO_4^-$,MoO_4^-	*Cell Rep. Physical Science*, **2022**,3, 100875
$ReO4^-$	UiO-66-NH_3^+	159	Cl^-, NO_3^-, SO_4^{2-}, PO_4^{3-}	*Inorg. Chem.* **2016,** 55, 8241−8243
$ReO4^-$	LDHs	130	N.D.	*Environ. Sci. Technol. Lett.* **2017**, 4, 316−322.
$ReO4^-$	SCU-101	217	NO_3^-, CO_3^{2-}, PO_4^{3-} ClO_4^-, SO_4^{2-}	*J. Am. Chem. Soc.* **2017**, 139, 42, 14873–14876
ReO_4^-	bis-PC 2(Cl)@MIL-101	362	NO_3^-	*ACS Cent. Sci.* **2020**, *6, 2354−2361*
ReO_4^-	TJNU-302	211	CO_3^{2-}, PO_4^{3-}	*ACS Appl. Mater. Interfaces,* **2020**, *12, 15246−15254*
MnO_4^-	SLUG-21	283	NO_3^-, CO_3^{2-}	*J. Am. Chem. Soc.*, **2010**, 132, 7202-7209.
MnO_4^-	UiO-66	94.29	N.D.	Inorg. Chem. **2019,** 58, 2899−2909
MnO_4^-	SCNU-Z1-Cl	**292**	N.D.	*Inorg. Chem.* **2019,** 58, 4, 2899–2909
MnO_4^-	SLUG-21	**292**	NO_3^-, CO_3^{2-}	*J. Am. Chem. Soc.* **2011**, 133,11110–1111
MnO_4^-	Compound-1	297.3	Cl^-, NO_3^-, Br^-, SO_4^{2-}	*Chem.Sci.* **2018,** 9 7874-7881
MnO_4^-	Ag(btr)·PF_6·0.5CH_3CN	163	NO_3^-, BF_4^-, ClO_4^-	*Inorg. Chem.* **2014**, 53, 12127-12134
MnO_4^-	IPcomp-6	281	Cl^-, Br^- NO_3^-, ClO_4^-	*Angew. Chem. Int. Ed.* **2022**,61, e2022033

MnO_4^-	Amberlite IR-120	4.9	N.D.	*Egypt. J. Aquat. Res.* **2015** 41, 2, 155–164
CrO_4^{2-} /$HCrO_4^-$	JU-111	105.4	NO_3^-, Br^-, Cl^-, HCO_3^-, F^-,CO_3^{2-}	*Angew. Chem. Int. Ed.* **2020**, 59,2–8
CrO_4^{2-}	IPcomp-3(200)	274.4	Cl^-, Br^-, NO_3^-, ClO_4^- SO_4^{2-}	*ACS Cent. Sci.*, **2020**, 6, 1534−1541
CrO_4^{2-}	Zn–Co-SLUG-35	68.5	NO_3^-, SO_4^{2-}	*Chem. Mater*. **2013**, 25, 647−652.
CrO_4^{2-}	IPcomp-6	243	Cl^-, Br^- NO_3^-, ClO_4^-	*Angew. Chem. Int. Ed.* **2022**,61, e2022033
CrO_4^{2-}	SBA	143	CO_3^{2-}, NO_3^-, SO_4^{2-}	*Inorg. Chem.* **2022**, 61, 51, 20824–20833
CrO_4^{2-}	MCMONs	279.92	N.D.	*Adv. Mater. Interfaces* **2018**, *5, 1800630*
CrO_4^{2-}	SCNU-Z1-Cl	126	N.D.	*Inorg. Chem.* **2019,** 58, 4, 2899–2909
CrO_4^{2-}	MgAl-LDHs	112	N.D.	*Water Res.*, ***2009***, 43, 3067−3075
CrO_4^{2-}	ZIF-67	5.88-13.34	N.D.	*Chem. Eng. J.* **2015**, 274, 238−246
CrO_4^{2-}	MOR-2	194	Br^-, Cl^-, HCO_3^-	*J. Mater. Chem. A* **2017**, 5, 14707-14719
CrO_4^{2-}	Lewatit MP 500	21.3	N.D.	*J. Hazard. Mater.* **2009**, 163 (1), 448-453
CrO_4^{2-}	BAC(10)	139.1	NO_3^-, Br^-, Cl^-, HCO_3^-, F^-, and CO_3^{2-}	*JACS Au* **2022**, 2, 7, 1669–1678
CrO_4^{2-}	CON-LDU3	232	PO_4^{3-}, NO_3^-, Br^-, Cl^-, HCO_3^-, F^-, CO_3^{2-}	*Adv. Mater. Interfaces* **2021**, 2100016
I_3^-	H_COF-7	1390	N.D.	*Angew. Chem. Int. Ed.* **2022**,61, e2022141
I_3^-	Cadmium(II)-triazole MOF	180	N.D.	*Chem. Commun.* **2011**, 47, 7185-7187
I_3^-	MBM - MOF	880	N.D.	*Angew. Chem. Int. Ed.* **2018**, 57,10148-10152.
I_3^-	THPS-C	926	N.D.	*Adv. Mater. Inter.*, **2019**, 6 , 1900249
I_3^-	TNHCP2	850	N.D.	*Sep. Purif. Techno.l* **2021**, *257, 117923*
I_3^-	TAPB-BPDA COF	988.17	N.D.	*React. Funct. Polym*, **159** (2021) 104806
I_3^-	PVDF/ZIF-8	73.33	N.D.	*Sep. Purif. Technol*., **238** (2020) 116488
I_3^-	NTP	429	N.D.	*ACS Macro Lett.*, **2016**, **5**, 1039
DCF^-	UIO-66	189	N.D.	*Chem. Eng. J.*, 2**016**, 284, 1406-1413
DCF^-	AC	76	N.D.	*Chem. Eng. J.*, **2016**, 284, 1406-1413
DCF^-	ZIF-8	100	N.D.	*Chemosphere* **2019**, 215, 524–531

DCF^{-}	CTAB-ZIF-67	60.58	N.D.	*New J. Chem.***2019**, 43, 11604-11609
DCF^{-}	CTAC	22.22	N.D.	*Water Res.* **2008**, *42*, 2873– 2882
DCF^{-}	Granular activated carbon	42.43	N.D.	*J. Clean. Prod.* **2018**, *181*, 145– 154
DCF^{-}	Modified chitosan/Fe3O4	151.0	N.D.	*J. Clean. Prod.*, **2018**, 172, 1025-1034
DCF $^{-}$	MCF	67	N.D.	*ACS Omega* **2022**, 7, 9, 7572–7584
DCF $^{-}$	Porous graphene	76	N.D.	*Chem. Eng. J.* ***2020***, *398, 125440*
DCF $^{-}$	Polypyrrole/ MWCNTs	45	N.D.	*Colloids Surf., A* ***2019***, *578, 123583*
DCF $^{-}$	CS/Fe3O4@TCOFs	333.33	N.D.	*Chem. Eng. J.*, ***2023***, *452, 139557*

N.D.= Not Done

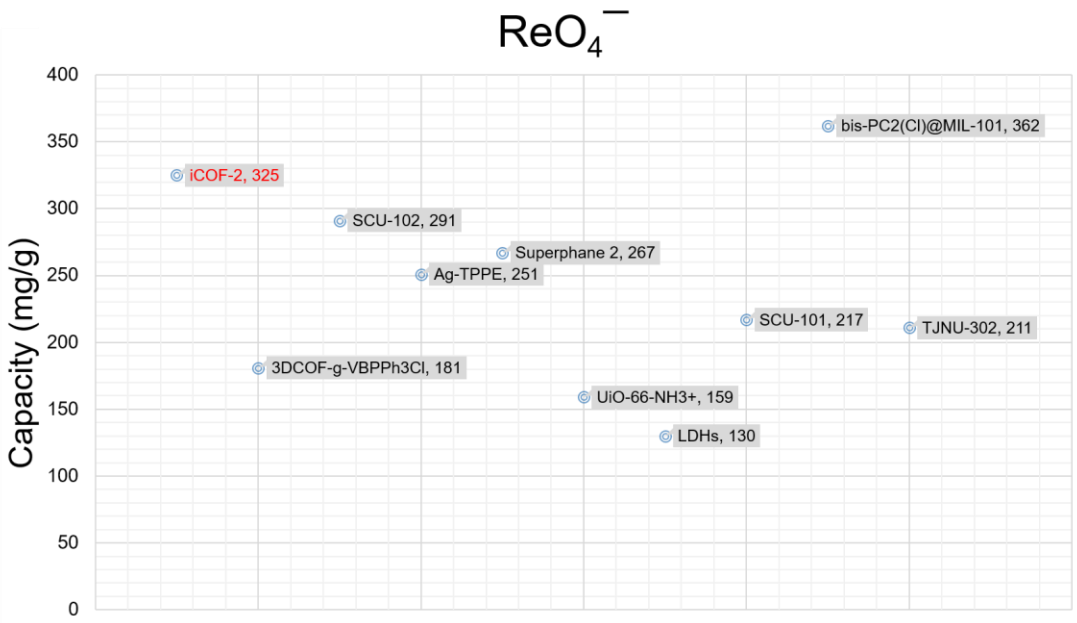
ReO_4^-
Capacity (mg/g)
400
350
300
250
200
150
100
50
0
bis-PC2(Cl)@MIL-101, 362
iCOF-2, 325
SCU-102, 291
Superphane 2, 267
Ag-TPPE, 251
SCU-101, 217
TJNU-302, 211
3DCOF-g-VBPPh3Cl, 181
UiO-66-NH3+, 159
LDHs, 130

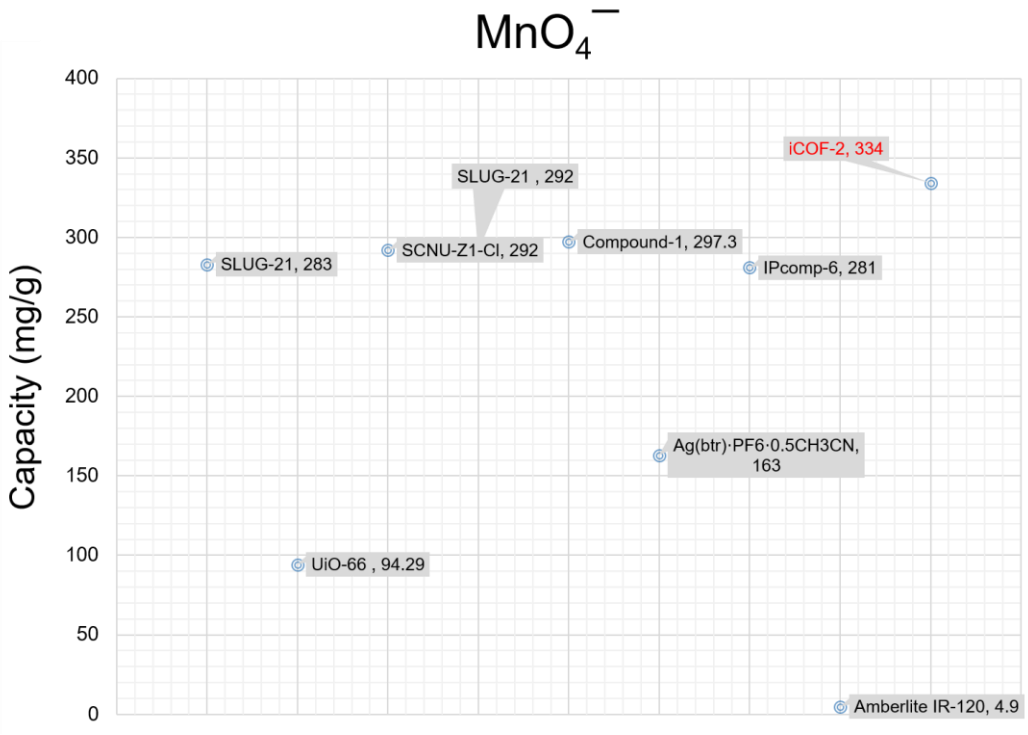
MnO_4^-
Capacity (mg/g)
400
350
300
250
200
150
100
50
0
iCOF-2, 334
SLUG-21 , 292
SCNU-Z1-Cl, 292
Compound-1, 297.3
SLUG-21, 283
IPcomp-6, 281
Ag(btr)·PF6·0.5CH3CN, 163
UiO-66 , 94.29
Amberlite IR-120, 4.9

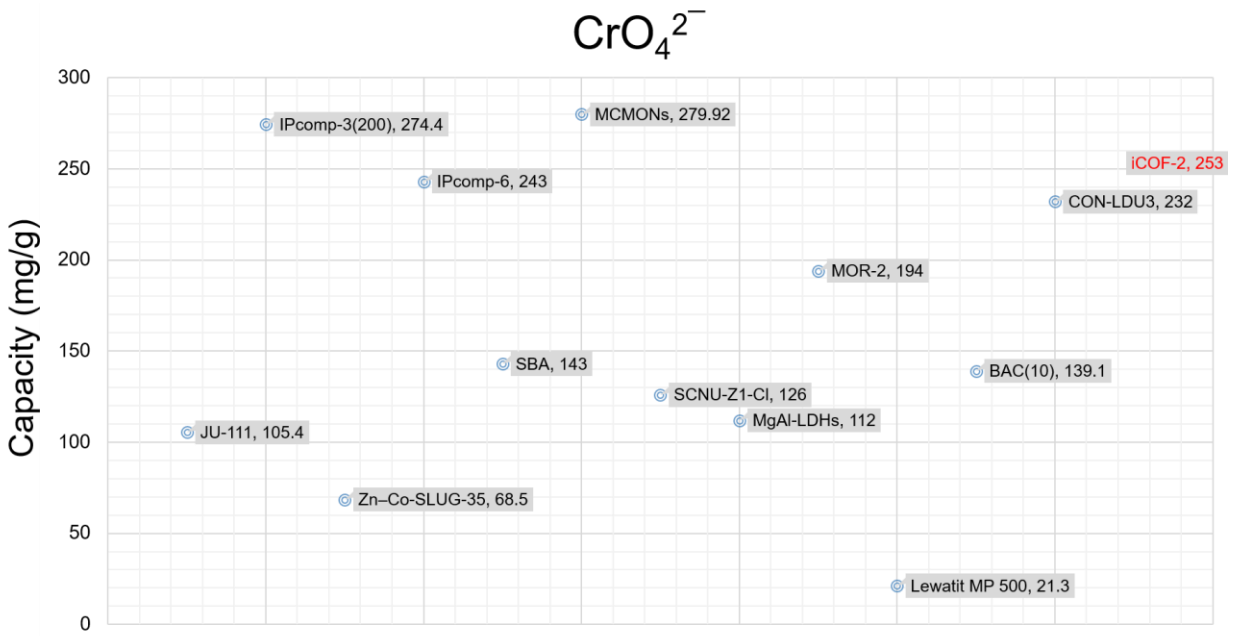
CrO_4^{2-}
Capacity (mg/g)
300
250
200
150
100
50
0
IPcomp-3(200), 274.4
MCMONs, 279.92
iCOF-2, 253
IPcomp-6, 243
CON-LDU3, 232
MOR-2, 194
SBA, 143
BAC(10), 139.1
SCNU-Z1-Cl, 126
MgAl-LDHs, 112
JU-111, 105.4
Zn–Co-SLUG-35, 68.5
Lewatit MP 500, 21.3

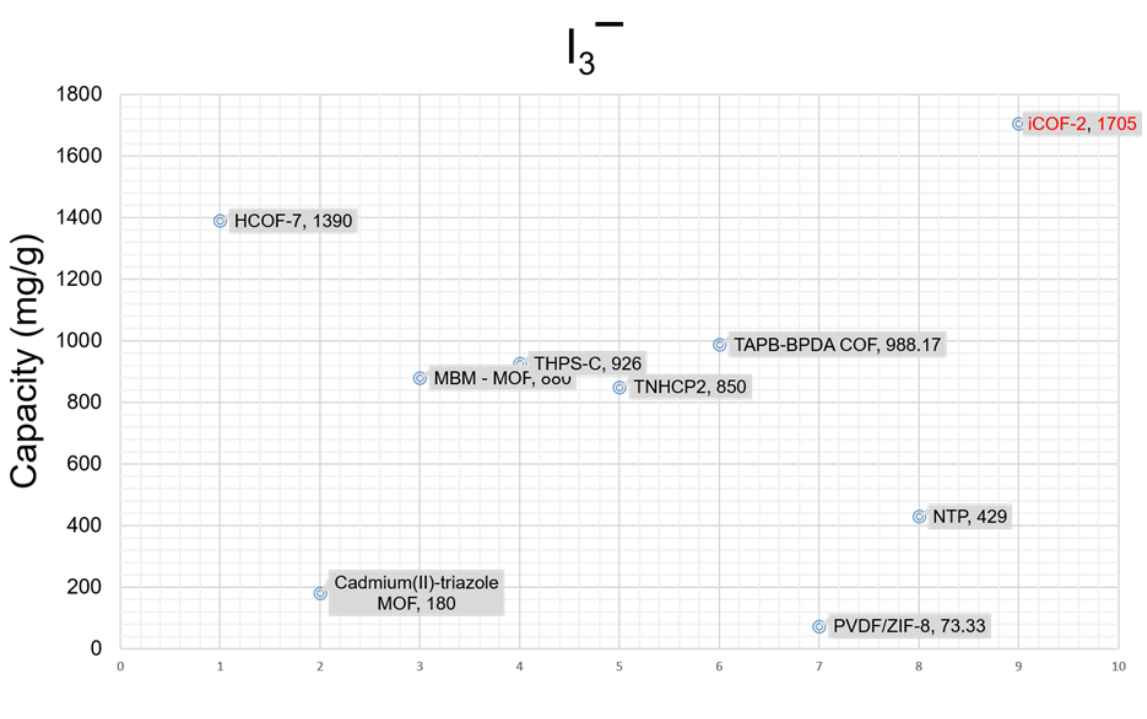
I_3^-
Capacity (mg/g)
1800
1600
1400
1200
1000
800
600
400
200
0
0
1
2
3
4
5
6
7
8
9
10
iCOF-2, 1705
HCOF-7, 1390
TAPB-BPDA COF, 988.17
THPS-C, 926
MBM - MOF, 000
TNHCP2, 850
NTP, 429
Cadmium(II)-triazole MOF, 180
PVDF/ZIF-8, 73.33

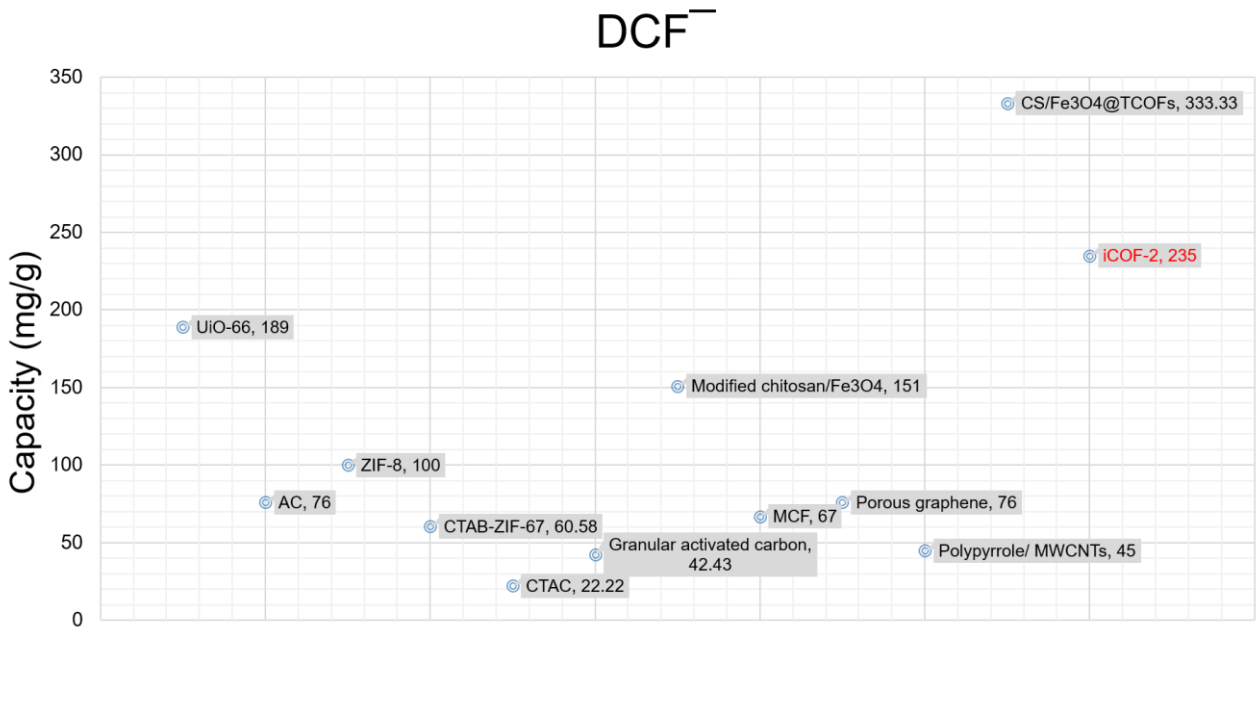

Fig. S32: Comparisons of iCOF-2 with other adsorbents

References

1. S. Haldar, D. Chakraborty, B. Roy, G. Banappanavar, K. Rinku, D. Mullangi, P. Hazra, D. Kabra and R. Vaidhyanathan, *Journal of the American Chemical Society*, 2018, **140**, 13367-13374.
2. S. Mitra, S. Kandambeth, B. P. Biswal, A. Khayum M, C. K. Choudhury, M. Mehta, G. Kaur, S. Banerjee, A. Prabhune, S. Verma, S. Roy, U. K. Kharul and R. Banerjee, *Journal of the American Chemical Society*, 2016, **138**, 2823-2828.